Imaging Mass Spectrometry Application in Colorectal Cancer Liver Metastasis Pathological Evaluation

Balqis Alabdulkarim
Department of Pathology
Faculty of Medicine
McGill University, Montreal, Canada

February 2016
A thesis submitted to McGill University in partial fulfillment of the requirements of the degree of Master of Science.

Table of Contents

ABSTRACT

Colorectal Cancer (CRC) is the second leading cause of cancer mortality in North America. Death from CRC is largely due to metastatic disease and the liver is the most common site of distant metastasis. Surgery when feasible carries the only chance of cure for Colorectal Cancer Liver Metastasis (CRCLM) patients. Post surgical resection further patient management and choice of adjuvant chemotherapy relies on pathological assessment of tumor grade. Multiple histopathologic assessment methods have been developed with variable correlation with patients' outcome. Until recently the Tumor Regression Grade (TRG) had the strongest correlation with patients' outcome. It scores lesions according to the ratio of fibrosis against the sum of viable tumor and necrosis. However with the widespread use of anti-angiogenic agents that causes necrosis as a form of response in the preoperative setting the modified Tumor Regression Grade (mTRG) evolved. It differentiates between two types of necrosis with different prognostic roles, Usual Necrosis (UN) and Infarct-Like Necrosis (ILN). Nonetheless pathological evaluation remains limited by its subjective nature. Our works describes the use of Matrix Assisted Laser Desorption and Ionization (MALDI) imaging mass spectrometry (IMS) to generate lipid signatures for different topographies. To do so we initially applied a semi-supervised histology driven approach to build our spectral library using an automated clustering method (k-means) and direct visual histological correlations (5-stain panel) on a training set (n=12). We identified six histologically correlated lipid signatures and further mined them for discriminate lipid markers. We used partial Least Squares-Discriminant Analysis (PLS-DA) to implement our spectral library on an independent validation cohort (n=40). Additionally, by dissecting out the lipid signatures we have identified single lipid moieties that are unique to UN and ILN that could potentially

be used as new biomarkers for assessing response to therapy. Using these signatures and lipid markers we obtained a histologically quantitative and objective mTRG score.

RÉSUMÉ

Le cancer colorectal (CCR) est la deuxième cause la plus importante de mortalité dérivée du cancer en Amérique du Nord. La mort causée par le CCR peut être attribuée à la métastase du cancer. Le site le plus fréquent de métastase éloignée de l'origine du CCR est le foie. Si cela est possible, la chirurgie donne la seule occasion de traitement pour les patients avec des métastases hépatiques du cancer colorectal (MHCCR). Les soins administrés après résection ainsi que le choix de chimiothérapie adjuvante dépendent de l'évaluation pathologique du grade de la tumeur. Plusieurs méthodes d'évaluation histopathologique ont été dévelopées, mais leurs corrélations avec les résultats des patients sont variables. Jusqu'à date, le « Tumor Regression Grade » (TRG) avait la plus forte corrélation avec les résultats des patients. Celui-ci marque les lésions selon la proportion de fibrose sur la somme de tumeurs viables et de nécrose. Pourtant, l'usage répandu d'agents anti-angiogéniques qui causent la nécrose lors de la période préopératoire a poussé le TRG à évoluer en TRG modifié (mTRG). Le mTRG différencie entre deux types de nécrose qui ont des rôles prognostiques différents : la Nécrose Commune (NC) et la Necrose qui ressemble à une infarctus (ILN). De plus, les évaluations pathologiques restent quand-même limitées par leur nature subjective. Le projet présenté dans ce mémoire décrit l'utilisation de l'imagerie de spectroscopie de masse (ISM) par Désorption/Ionisation Laser assistée par Matrice (MALDI) afin de définir les signatures lipidiques signatures pour des topographies différentes. Nous avons initialement appliqué une approche histologique semi-supervisée afin de construire notre banque spectrale par une méthode automatique de classification (k-means) et des corrélations histologiques visuelles directes (panneau de 5 couleurs) sur une série d'échantillons préparatoire (n=12). Nous avons identifié six signatures lipidiques qui sont mises en corrélation par histologie et puis, nous les avons exploitées afin de découvrir des marqueurs lipidiques discriminants. Nous avons utilisé la méthode d'analyse « Partial Least Squares-Discriminant » (PLS-DA) afin de mettre en

place notre banque spectrale sur une cohorte de validation indépendante de 40 patients. De plus, en analysant les signatures lipidiques, nous avons identifié des fractions lipidiques uniques distinguant les NC et les ILN, qui peuvent potentiellement être utilisées comme biomarqueurs pour évaluer la réaction au traitement. En utilisant ces signatures et marqueurs lipidiques, nous avons obtenu un score de mTRG quantifié par histologie et objectif.

ACKNOWLEDGMENTS

I would like to extend my appreciation to my supervisor Dr. Peter Metrakos for offering me the chance to pursue my graduate studies and his guidance throughout the years. I would like to express my heartfelt gratitude to Dr. Anthoula Lazaris for enlightening me with her knowledge, and for her guidance that spanned beyond my academic trajectory and taught me valuable lessons in life.

To my advisory committee members, Dr. Pierre Chaurand my deepest thanks for his insightful comments and his ultimate support in helping me realize this thesis and to Dr. Miguel Burnier for his constant encouragement.

Special Thanks to Heath Patterson for his work and collaboration in developing this study. Thanks to Eve Simoune and Husaam AlAmri for their valuable comments and suggestions. Many thanks to Stephanie Petrillo, Loutfi Amri, and Ayat Salman for their help and support.

My appreciation and gratitude to Sossy Sahakian and Evette Yassa for their invaluable friendship and endless support.

Last but not least, I would like to extend my warmest appreciation to my parents for believing in me and their tremendous pride for my achievements. My sibling for setting the bar too high. My nieces and nephews for being their adorable selves.

PREFACE

This dissertation is based on collaborative work between Heath Patterson at the University of Montreal and myself. MS data treatment including normalization, smoothing and peak picking was done strictly by Patterson. Clinical data collection including assessing radiological and pathological response was done strictly by me (validated by a licensed radiologist and pathologist respectively). Correlations between clinical data and lipid expression and data mining was performed by the both of us.

1. INTRODUCTION

1.1 Colorectal Cancer and Liver Metastasis Burden

Colorectal cancer is a major cause of cancer morbidity and mortality worldwide[1]. In North America it constitutes 8.4% of all cases of cancer and is the second leading cause of cancer mortality[2,3]. As local disease is promptly controlled and dealt with surgically, death is largely due to distant metastasis[4]. This is observed with five year overall survival rates of metastatic disease (stage IV) being around 13.1% only as opposed to 90.1% and 70.8% for local and regional disease (Stages I to III) recepectively[2]. The liver is the most common site of metastatic disease due to the nature of the portal circulation that drains the blood from the digestive tract directly to the liver. About 25% of patients will be burdened with liver metastasis at primary presentation (synchronous) while over half of them will present with it at some point thereafter[5]. Synchronous presentation is associated with worst outcome[6]. Furthermore, around third of stage IV disease patients will have the liver as the sole site of metastasis[7].

1.2 Colorectal Cancer Liver Metastasis Management

1.2.1 Surgical Intervention

Surgical intervention when feasible carries the only chance of cure and long-term survival for colorectal cancer liver metastasis (CRCLM) patients, with five year overall survival rates for patients undergoing surgical resection observed at 47%[8,9]. Historically, surgical resection was limited by many factors including multiple lesions, proximity to major vessels and hilar adenopathay[10]. In today's clinical practice, this is no longer the case. Nevertheless, the

majority of patients are burdened by extra-hepatic disease at presentation thus deemed unresectable and will consequently be offered palliative chemotherapy[11]. Alternatively, these patients can undergo resection with limited improvement in survival rates if the extra-hepatic disease can be similarly dealt with as well. However a vigilant patient selection process needs to be practiced[12].

1.2.1.1 Conditions for Resection

Currently, two conditions need to be satisfied for a patient to be considered for surgical intervention. One of which is microscopically clear surgical margins (R0)[13]. Based on preoperative imaging tumor free margins should be thought feasible, this will be further verified by intraoperative ultrasound. The width of free margins has been controversial however there is agreement that free margins of any width carry significantly better outcome than involved margins whether microscopically or grossly (R1 and R2 respectively)[9,14]. The second condition is a sufficient future liver remnant (FLR) along side the preservation of two adjacent segments and vessel integrity[15]. FLR is the volume of the remaining liver after resection, it is assessed through preoperative imaging studies using computed tomography (CT) in relation to body weight or body surface area[16]. Up to 80% of the liver can be safely removed, as a FLR of 20% is adequate in normal otherwise healthy liver[17]. However if chemotherapy induced hepatotoxicity is suspected this is further increased to roughly 30-40% as well as in cases of liver injury due to steatosis among other conditions[17]. A small FLR has been correlated with post-hepatectomy liver failure (PHLF), a condition associated with postoperative mortality and defined as a failure of one or more synthetic and excretory liver functions[16,18]. To avoid this, portal vein embolization (PVE) can be attempted in those patients[19]. It is a minimally invasive procedure that induces atrophy to the tumor burdened

lobe and hypertrophy to the counter-lateral lobe by embolization of portal venous branches[20]. In addition, it is contraindicated in patients with sufficient FLR as it promotes tumor progression despite atrophy[21,22]. Another conversion modality for initially unresectable tumors is neoadjuvant (preoperative) chemotherapy or as appropriately called in this case, conversion chemotherapy[22,23].

1.2.2 Neoadjuvant Chemotherapy

Neoadjuvant chemotherapy can be similarly given to initially resectable patients to improve postoperative outcome[24,25]. Chemotherapeutic agents commonly used in these regimens include a base of Folinic acid and Flurourcil (5-FU), a thymidylate synthase inhibitor, along with Oxaliplatin, a cytotoxic agent, and/or Irinotecan a topoisomerase 1 inhibitor (referred to as FOLFOX, FOLFIRI and FOLFOXIRI respectively)[26-29]. More recently, Bevacizumab, an angiogenesis agent that inhibits vascular endothelial growth factor A (VEGF-A), has been increasingly used along side these regimen as well[30-34]. In some centers Cetuximab, an epidermal growth factor receptor (EGFR) inhibitor, is also being used as first line therapy in selected patients[35,36].

1.2.3 Response to Chemotherapy Assessment

Patient response to chemotherapy is assessed through radiological imaging (CT or MRI), which necessitates that baseline scans be performed and follow up scans be repeated in 8 weeks to 3 months[37,38]. A widely clinically used method is the Response Evaluation Criteria in Solid Tumors (RECIST), it assesses response based on size changes of target lesions where a decrease in size of >30% is considered a response[39]. This method of assessment is limited by size changes and might underestimate response when using anti-angiogenic agents (e.g.

Bevacizumab) where it elicits central necrosis and consequently increases lesion size as a form of response[40]. The modified RECIST (mRECIST) developed to assess Hepatocellular Carcinomas (HCC) treated by Sorafenib, an inhibitor of vascular endothelial growth factor (VEGFR), which causes central necrosis as a treatment response as well, tackled this limitation[41]. It assesses response according to size changes of viable tumor in target lesions by using contrast enhanced dual phase imaging, instead of the whole lesion size[41,42]. However its application beyond HCC are yet to be investigated. A single study comparing RECIST and mRECIST in relation to pathological response in CRCLM found neither to be predictive of residual viable tumor burden[43]. Alternatively, the Morphological Criteria that uses CT scans to assess changes in attenuation morphology is found to have a statistically significant association with pathological response and patient outcome. However, its application in clinical settings is not as widespread as that of RECIST[44].

1.2.4 Patient Prognostication and Outcome

Post resection, patient prognostication plays a major role in further patient management including choice and duration of adjuvant chemotherapy agents. Traditionally, clinical scores were used to predict patient's outcome[45]. These include the preoperative clinical risk score (CRS) that takes into account five clinical criteria: primary tumor nodal status, disease free interval, number of lesions, size of the largest lesion, and preoperative Carcinoembryonic Antigen (CEA) serum levels[46]. The latter is a glycoprotein involved in cell adhesions; it serves as a non-diagnostic tumor marker for CRC and CRCLM that can also be elevated in other conditions including various gastrointestinal tumors[47]. CRS along with other clinical scores were capable of stratifying patients into high and low risk groups by which predicting patients' outcome and suitability for surgical intervention[46,48]. However, with the relatively recent widespread use of neoadjuvant chemotherapy, these scores are considered rudimentary

and no longer correlate well with patient outcome[45,49]. On the other end of the spectrum, molecular biomarkers have long been described in CRC. These include KRAS mutation, a point mutation in codon 12 and 13 that occur in up to 40% of CRC patients[50]. It is a well-established predictor of resistance to Cetuximab in stage IV disease[51]. Other drug targets have similarly been described in the last decade however they are yet to be implemented in clinical practice[52]. KRAS mutation also plays a predictive role in patient survival with local and regional disease, however it is not well described in metastatic disease[53,54]. Another clinically established molecular biomarker is Microsatellite-Instability (MSI); it serves as a predictor of benefit from Fluorouracil based chemotherapy[55]. In the era of personalized medicine these molecular biomarkers will be further applied in the clinical setting, but as it stands now they are of limited applications as drug targets. In the midst of the outdated clinical scoring systems and the not yet well-implemented molecular biomarkers is the pathological grading and response. Pathological assessment allows for actual tumor burden evaluation as the amount of viable tumor alone has been well correlated with patient outcome[56].

1.2.4.1 Pathological Evaluation and Response

Pathological evaluation not only predicts patient outcome by assessing response to preoperative chemotherapy it also evaluates surrounding normal liver parenchyma for chemotherapy associated toxicity that could lead to morbidity, further driving the choice of future chemotherapy and management[57,58]. It additionally assesses tumor margins, an important independent prognostic factor, as patients who received downsizing perioperative chemotherapy were observed to recur at the margins.[59] Pathological grading systems have been developed to address this with variable correlation with survival[56,60-63]. The Tumor

Regression Grade (TRG) demonstrates a good correlation with patient outcomes including overall and disease free survival[62,64]. It takes into consideration the degree of fibrosis and necrosis in relation to tumor viability, in which fibrosis is considered a positive indicator and necrosis a negative indicator of response[62]. However, with the widespread use of Bevacizumab and other anti-angiogenic agents, the Modified Tumor Regression Grade (mTRG) emerged[65]. mTRG differentiates between two types of necrosis **(**Fig1.1) seen in resections; usual necrosis (UN), typical of tumor progression, and infarct-like necrosis (ILN), a response to treatment, whose presence has been associated with favourable prognosis[65].

A limitation that still remains is subjectivity. Pathological evaluation and grading is done through 'eye-ball' semi-quantitative estimates, as a cell-count approach is not feasible in this setting. Inter- and intra-pathologist variability has been observed in literature[66,67]. A complementary objective histologically quantitative technical approach can further enhance pathological synoptic reporting[68].

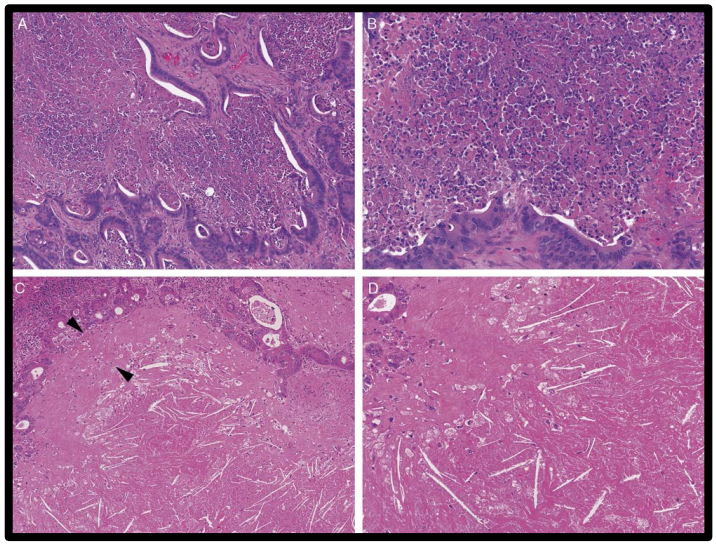

Figure 1.1 Types of Necrosis. **A** and **B** featuring Usual Necrosis, surrounded by viable tumor and characterized by its patchy distribution and nuclear debris. **C** and **D** Featuring Infarct-Like Necrosis, characterized by larger confluent areas and walled off by desmoplastic-like ring (black arrows). [65]

1.3 Imaging Mass Spectrometry

Imaging Mass Spectrometry (IMS) is a mass spectrometry (MS) technique that allows direct visualization of molecules on tissue sections by providing chemical and spatial information[69]. In brief, MS is an analytical chemistry modality that uses an ion source to identify molecules based on their mass to charge ratio (m/z)[70-72]. A Mass Spectrometers is composed of three main parts, an ionization source, an analyzer and a detector (Figure.1.2)[73]. Both the ionization source and analyzer can differ according to which specific device is used although the basic concept remains unvaried[74]. The raw data generated by spectrometers is a mass spectrum, a plot of ion intensity (abundance) against *m/z* (Figure1.3)[73]. The analyte is the biomolecule of interest and will be detected as a gas-phase ions, it can be proteins or lipids among other targets[75,76]. When this is performed on an intact tissue section it is known as IMS.

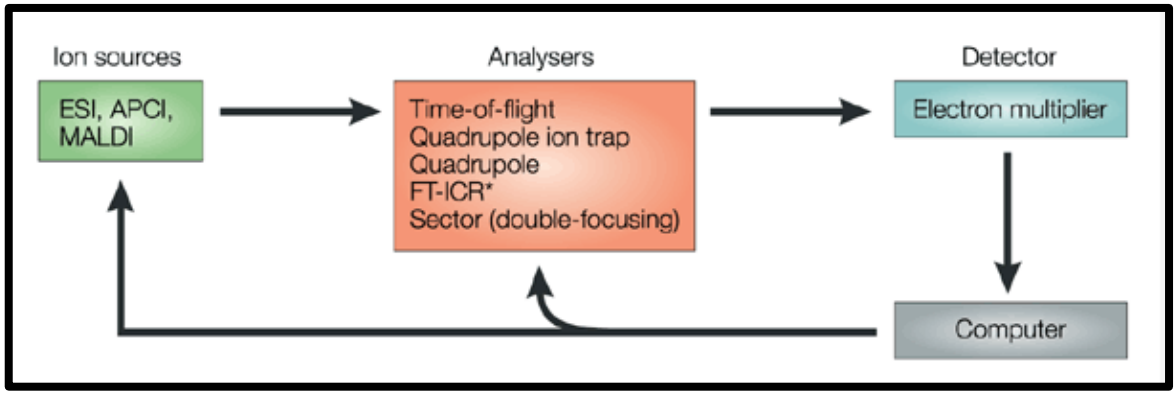

Figure 1.2 Mass Spectrometry workflow. Ion sources can be coupled with different type of mass analyzers. [73]

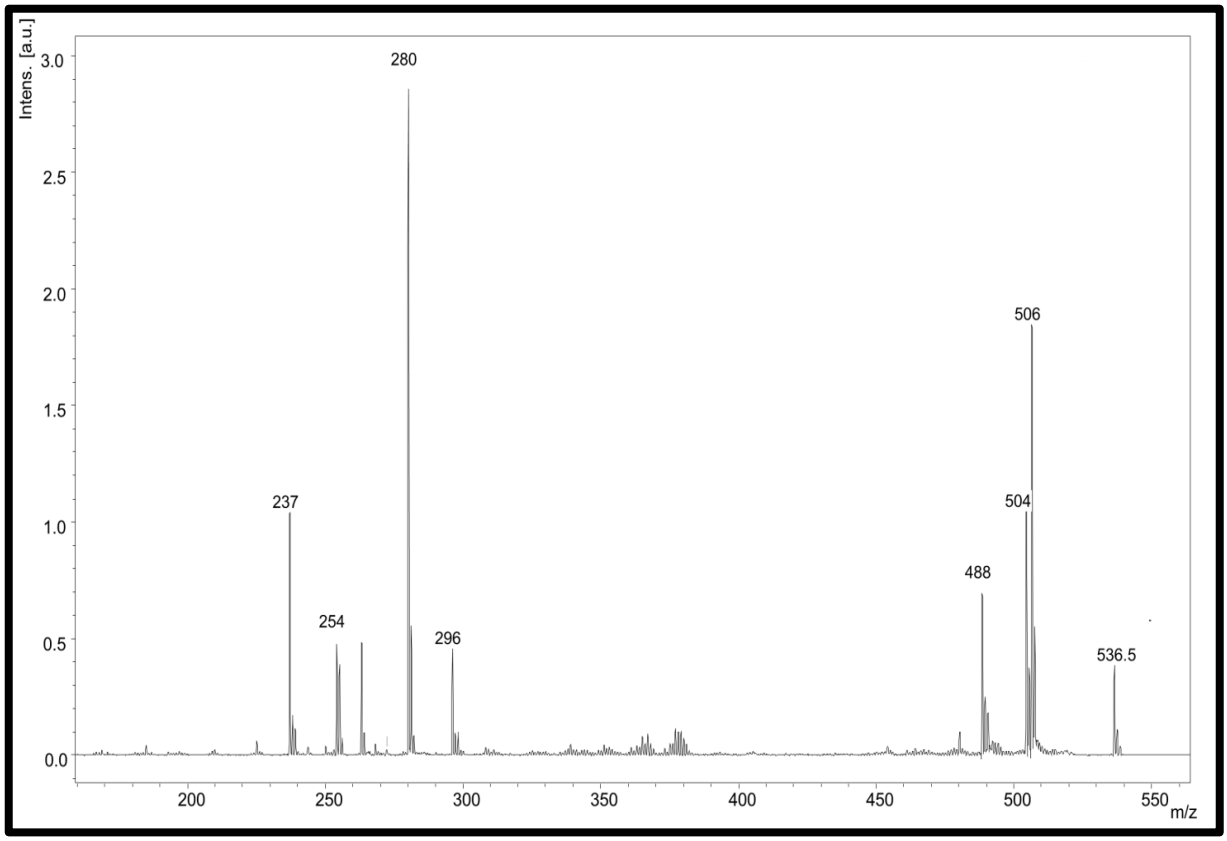

Figure 1.3 Mass Spectrum. An example of a mass spectrum from our data.

1.3.1 Matrix Assisted Laser Desorption and Ionization

Matrix Assisted Laser Desorption and Ionization (MALDI) is the most commonly used IMS method[77]. It captures mass spectra at defined 2-D positions across an intact tissue and reconstructs data into ion maps that reflect molecular distributions[78,79]. Matrix application will result in matrix-analyte co-crystal formation[80]. The choice of matrix is extremely important and depending on the analyte, the type of matrix and the method of its application will differ[81]. Matrices are small organic acids that allow uniform desorption across the sample by absorbing the ionizing laser first, then in turn ionizing the sample[80]. A pulse UV laser is used to create gas-phase ions of the analyte (Figure1.4) [81]. MALDI can work in both positive and negative modes to detect positive and negative ions respectively, therefore allowing the identification of larger set of molecules. The choice of matrix also plays a role here as not all matrices can be used in both modes[82]. In MALDI IMS the gas-phase ions are

formed through protonation and deprotonation, which is the addition or loss of a proton or more instead of an electron as seen by most preceding spectrometers[73]. Moreover, it preforms soft ionization, which means that the molecules are transferred intact into the gas-phase form without fragmentation[83]. This is advantageous, as molecules do not require reconstruction to be identified; furthermore because of the nature of the ionization the sample is not exhausted and can be used for downstream staining[68]. Once the m/z(s) of interest are chosen, established online databases can be used to inform about their identity[84,85]. Often times the identity of molecules need to be further confirmed, in that case Tandem Mass Spectrometry (MS/MS) can be utilized[86]. In MS/MS molecules are purposefully fragmented to ascertain their identity. This is done in two steps, the first to isolate the m/z of interest, which is known as the parent molecule or precursor ion. The second is to fragment the parent molecule and identify its components[73]. The mass analyzer most commonly coupled with MALDI is the Time of Flight (TOF). It operates on the simple concept that given that all ions travel the same distance to the detector and are accelerated at fixed potential, smaller ions with lower m/z will achieve higher velocity and consequently detected at an earlier time[87].

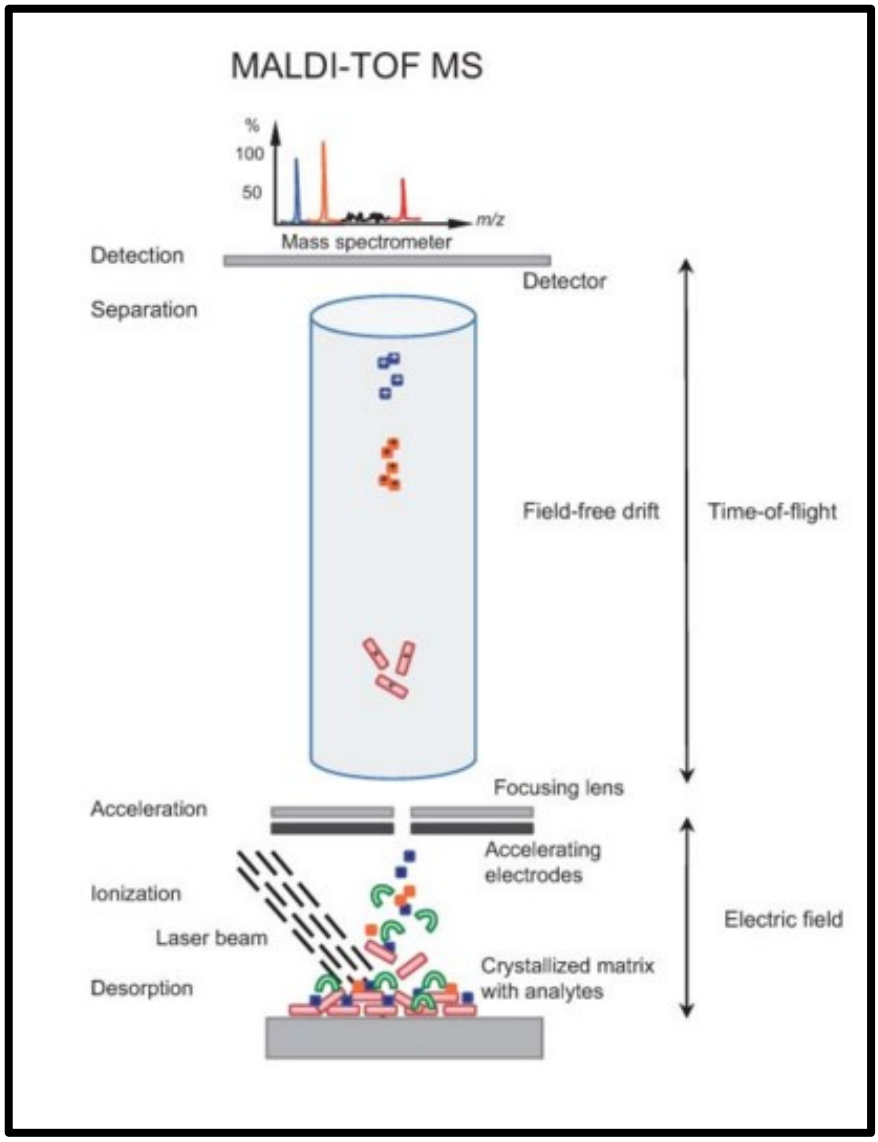

Figure 1.4 MALDI IMS Schematic Representation. Laser pulse charges the analyte-matrix crystals into gas phase ions that are in turn accelerated through the mass analyzer (TOF) to the detector. [88]

1.4 Lipids

1.4.1 Lipidomics

Lipdiomics is an emerging field pertaining to mapping of the lipidome and investigating its interaction with other biomolecules[89]. Unlike the other classes of biomolecules, lipids do not share a common chemical structural feature rather they are defined by their water insolubility[90]. Lipidomics, introduced recently after genomics and proteomics, owes its

relatively rapid expansion to advances in analytic chemistry, specifically mass spectrometry[91]. These allowed detailed description of the cell's lipidome from classes to subclasses to the individual molecular species. It also facilitated lipid metabolism investigations as well as describing lipid-lipid and lipid-protein interactions[92]. LIPID MAPS online database was formed soon thereafter to deal with the massive amount of data generated and ease international collaboration[84].

1.4.2 Phospholipids

Phospholipids are a heterogeneous class of lipids characterized by a polar hydrophilic head and a hydrophobic tail, their amphipathic nature facilitate basic membrane function[93]. Phospholipids play multiple roles in the physiological cellular state, including their involvement in second messenger signalling and their function as cellular energy reservoirs[94]. One of the most well recognized functions of phospholipids is their role in cellular architecture as they form the plasma lipid bilayer[95]. The majority of cellular lipids are mainly synthesized in the Endoplasmic Reticulum (ER)[96]. Suitably, to facilitate its function in the insertion and transport of newly synthesized lipids and proteins the ER membrane phospholipids themselves are loosely packed[97]. This is achieved by rapidly transporting sterols and complex sphingolipids to other organelles and highlights how the type of phospholipids and their concentrations have to be fine-tuned to meet the requirements of physiological function[97,98]. Other organelles such as the Golgi and Mitochondria are involved in lipid synthesis to a lesser extent[99,100]. Lipids synthesized in the Golgi are almost invariably designated for the plasma membrane. Despite the fact that the plasma membrane is not directly involved in lipid synthesis, it contributes to lipid production through phospholipids turnover such as sphingomyelin (SM) synthesis from plasma membrane ceramides[101]. The plasma lipid bilayer complexity is further increased by its asymmetrical nature due to

variance in phospholipid distribution across its inner and outer leaflets, which imparts different functional characteristics[102,103].

1.4.3 Lipid Dysregulation in Cancer

In cancer processes aberrant lipid synthesis has been observed as early as 1953, when it was demonstrated that tumor tissue had increased *de novo* lipogenesis, comparable to that of liver tissue[104]. This was further propagated by the discovery that OA-519, a negatively prognostic breast cancer tumor marker, was in fact Fatty Acid Synthase (FASN)[105]. An increase in fatty acid (FA) *de novo* synthesis is necessary to maintain the membrane production needed by the proliferating tumor[106]. Most of these newly synthesized FAs are predominantly designated for phospholipid production and consequently incorporated in the plasma lipid bilayer[107]. These findings were validated by the upregulation of upstream cellular pathways in cancer cells[108]. This led to mining lipogenesis pathways for antitumor drug targets[109,110]. Beyond the aforementioned role that lipids play in the proliferating cancer cell, there is evidence of its involvement in malignant transformation[111]. As the cells move from the physiological up take of free FAs and lipoproteins to the pathological increase in *de novo* synthesis the lipid bilayer saturation increases rendering the cancerous cell more resilient to oxidative damage[112]. The dynamic and complex nature of lipids and especially phospholipids metabolism in health and disease makes them attractive biomarker candidates.

1.5 MALDI IMS Lipidomics Clinical Applications

1.5.1 Applications in Cancer Research

Imaging Mass Spectrometry applications in clinical studies have long been performed. It originally started with bacteriology studies but soon was utilized in other fields[113]. Proteins

and peptides have been the major culprit in clinical studies. This is in part due to the availability of formalin fixed paraffin embedded (FFPE) tissue samples in clinical research as opposed to fresh frozen samples required for lipid analysis[114]. However, more recently lipids are being investigated for clinical applications as well[115,116]. In cancer research MALDI IMS has been used mainly for prognostic, predictive and diagnostic biomarker development. Clinical lipidomic studies utilising IMS in cancer are scarce compared to those of proteomics, nevertheless they are currently gaining growing attention as a promising field for biomarker discovery. A recent study concerning prostate cancer used tissue from resection specimens to compare viable tumor to adjacent normal epithelium[117]. They successfully identified a single lipid (lysophosphatidylcholine (LysoPC) (16:0 OH)) as an independent predictor of biochemical recurrence after radical prostatectomy[117]. Using a similar approach in two different non-small cell lung cancer cell lines (PC9, PC9R) rather than tissue section to assess response to therapy (responsive vs. resistant respectively) also revealed difference in lipid expression[118]. Furthermore, its applications in diagnostics are also being tackled where a thyroid cancer study using MALDI IMS on tissue section of malignant and benign thyroid tumors[119]. They identified phospholipids including phosphatidylcholine (PC) and sphingomyelin (SM) species that were expressed differently. This was taken a step further by finding these lipid signatures in the serum of these patients with sufficient specificity and sensitivity rendering it more applicable to the clinical setting[119].

1.5.2 Application in Colorectal Cancer and Liver Metastasis

A couple of studies regarding CRC using MALDI IMS lipidomics have been conducted. The earlier of the two was a feasibility study assessing the suitability of MS as a pathology tool using CRCLM tissue sections[120]. In a supervised histology-driven approach two Regions of

Interest (ROI) were chosen according to pathologist annotation; one of viable tumor area and the other of adjacent normal tissue. By comparing the lipid profiles of the two regions they were able to identify a tumor specific SM ((16:0)+Na) at 725 *m/z*[120]. The second study was performed on CRC specimens where a supervised histology-driven approach was also performed. However, three ROI were chosen here pertaining to cancer tissue, adjacent normal and distant normal tissue[121]. Discriminant analysis was performed to investigate the metabolic field effect of the tumor microenvironment (TME). The analysis identified three ions differentially expressed in tumor tissue compared to non-tumor (adjacent and distant) at m/z 478.3, 504.3 and 760.6, which was later identified by MS/MS to be LysoPC (16:0), LysoPC (18:1) and PC (16:0/18:1) respectively. By plotting their expression according to class (tumor, tumor-adjacent, and tumor-distant), a slight overlap between tumor and tumor-adjacent spectra expression was observed further supporting the TME field effect[121,122]. TME was also investigated in CRCLM in a MALDI IMS proteomics study where three zones were identified (peritumoral, rim and center) according to their peptide expression[123]. Both lipidomic studies where performed only in positive ion mode and were limited by a small sample number (n=1 and n=12 respectively)[120,121].

1.6 Objective

In this Study, we describe MALDI IMS lipidomics applications in CRCLM management. The main focus of the study is to turn the subjective semi-quantitative pathological assessment into an automated objective histologically quantitative one. To do so we used a training-set of 12 fresh frozen CRCLM resection samples to build a spectral library that identifies histology based molecular signatures (phospholipids) and validated these signatures

on another 40 samples. We further explored its clinical application by generating IMS derived mTRG and correlating it to pathologists' mTRG.

2. METHODS AND MATERIALS

2.1 Tissue Procurement

Tissue specimens were procured between November 2011 and July 2014 from 52 liver resections for 50 patients (two patients underwent staged resections). Through the McGill University Health Center (MUHC) Liver disease Bio-bank (LDB) informed consent was obtained (LDB: MUHC research ethics board approved protocol:SDR-12-174). Post pathological confirmation of cancer diagnosis and surgical margins specimens were immediately banked and frozen within 30 minutes as per LBD banking protocol. Specimens were allowed to cool down on ice briefly for 10 minutes before getting immersed in isopentane at -45ºC for 10 to 15 minutes for complete freezing. Next, the tissue was wrapped in foil and stored at -45ºC until sectioning.

2.2 Clinical Data Collection

Full clinical data for each patient was collected through medical records and hospital database (OACIS) used at MUHC including review of operative, radiological and pathological reports as well as clinical transcriptions. Data collected included patient demographics (age and sex), primary disease data (date of diagnosis, type of presentation, location within the proper colon, sigmoid colon or rectum, management modalities, date of surgical intervention if applicable, TNM classification, and lymphovascular involvement), liver metastasis data (type of presentation -synchronous vs metachronous-, date of diagnosis, type and date of surgical intervention, location of metastasis (lobe and segment), size and number of lesions, degree of differentiation, and PVE status), chemotherapy details (type of agents, number of cycles, date of first and last cycles, and radiological response according to

RECIST), relevant laboratory and biomedical results (CEA levels: pre-chemo, pre-op and post-op), personal and family history of cancer, and the presence of co-morbidites.

2.3 Survival Analysis and Statistics

Overall survival (OS) and disease free survival (DFS) were calculated for each patient. Overall survival was calculated from the date of metastasis diagnosis until the date of last follow-up. Disease free survival was calculated from the date of surgical intervention when complete resection was achieved to the date of recurrence or last follow-up if patient remains in remission. OS and DFS analysis was performed using the Kaplan-Meier survival analysis for the full cohort, training set and validation set. Further, survival analysis was done for pathological response groups (major, partial and minor) according to two independent pathologists grading as well as our developed pathological based IMS grading. Kaplan-Meier survival analysis curves were generated and significance was assessed using the log-rank test. Significance was set at $P \leq 0.05$. Statistical analysis was performed with both Prism 6 and JMP 11 for Mac OS.

2.4 MALDI-IMS Data Treatment

FlexImaging 4.1 (Bruker Daltonics, Billerica, Massachusetts) was used to export data to .imzML format[124], a flexible data format developed for IMS that allows the comparison of data from different instruments by applying identical parameters, for downstream data treatment in R environment using MALDIquant package[125]. Total Ion Current (TIC)[126] global normalization was performed next. This step is crucial as mass spectra of different samples are not always quantified within the same amplitude range and therefore not comparable

without normalization[126]. For peak picking process, smoothing was done according to Savitzka and Golay algorithm[127]. This is done to avoid false-positive peaks. Peak picking was performed at a single-to-noise ratio of 3.0.

2.5 Clustering and Data Mining

Using Cardinal MSI package[128] in R environment, spatially aware K-means (k=7) algorithm was performed and collated to build our spectral library. K-mean is an approach to segmentation that incorporates spatial information directly into the clustering method[129]. Partial Least Squares – Discriminant Analysis (PLS-DA) was next performed to implement spectral library using the mixOmics package[130]. Receiver operator curve analysis was done using ROCR package[131] in the R environment to identify histology specific discriminate lipids.

2.6 Tissue Sectioning

Serial sections 10-12 μm thick were cut using a Hacker/Bright cryostat (Hacker Instruments & Industries Inc., Winnsboro, CA) and stored in tightly closed box at -40°C to be used later for staining. Two serial sections of each sample were placed on special indium-tin-oxide (ITO) coated glass slides (Delta Technologies, Stillwater, MN) to be used for imaging mass spectrometry. ITO slides were either stored at -80°C or analyzed immediately. The rest of the slides were fixed for 60 minutes in 4% formaldehyde dissolved in 0.1 M phosphate buffer at pH 7.2 before staining.

2.7 Histological Characterization

Using serial sections of each specimen a histological panel of 5 stains was built for the training set (n=12) to serve as a comparative assay for correlating IMS data with the different histologies in our specimens. The panel included: Apolipoprotein F (ApoF) in-situ hybridization (ISH) (a hepatocyte-specific stain that defines regions of liver adjacent to the tumor area), phospholipid transfer protein (PLTP) ISH (showing macrophages aggregation within or around the tumor), alcian blue (AB) (staines mucin within the tumor), haematoxylin and eosin (H&E)(a principle stain for general histology), and Ki67 immunostaining to identify viable tumor areas. Only H&E staining was performed for the validation set (n=40) on a serial section to validate topographies retrospectively after identifying them using lipid signatures.

2.7.1 H&E Staining

Fixed tissue sections were immersed for 2 minutes in hematoxylin solution (Sigma, cat. #H3136) prepared according to the manufacturer instruction and filtered before use. Tissue sections were then washed for 10 minutes under running tap water. Then, sections were stained for 3 minutes in eosin Y solution (Fischer cat. #E-511) prepared according to the manufacturer directive. Following staining, sections were transferred directly to 95% ethanol, then dehydrated in a series of alcohol baths of 3 minutes each (one 95% and two 100% ethanol baths), cleared with 3 xylene baths of 2 minutes each and finally cover slipped with permount[132].

2.7.2 Alcian Blue Staining

Fixed tissues were washed in water for 5 minutes and stained for 45 minutes in 1% alcian blue 8GX (Sigma, cat. #05500) in 0.1 M hydrochloric acid solution at pH 1.0. As described for H&E staining, following staining, sections were transferred directly to 95% ethanol, then dehydrated in a series of alcohol baths of 3 minutes each (one 95% and two 100% ethanol baths), cleared with 3 xylene baths of 2 minutes each and finally cover slipped with permount[133].

2.7.3 In Situ Hybridization

In situ hybridization (ISH) was performed with [35S]-labeled riboprobes synthesized in vitro from DNA Templates at cytochrome.inc. Briefly, mouse Apolipoprotein F (ApoF, GenBank AF411832.1) DNA template of 675 bp was produced by PCR using sense gataccagatgcagacctca and antisense gttcgtcgttgttgacaaga primers. Human phospholipid transfer protein (PLTP, GenBank NM_006227.3) DNA Template of 884 bp was produced using GAAGAGCGGATGGTGTATGT (sense) and TGGTGGACGGACTGTAATTG (antisense) primers. Sequences recognized by SP6 Polymerase (5′-GCATTAATTTAGGTGACACTATAGAAGCG...-3′) were attached to antisense and T7 Polymerase (5′-GCGCTATAATACGACTCACTATAGGGAGA...-3′) to sense primers. Following hybridization, the results were visualized by x-ray film autoradiography showing anatomical level topography and emulsion autoradiography showing cellular level ISH labeling[134,135].

2.7.4 Ki67 Immunohistochemistry (IHC)

Rabbit monoclonal-antibody (cat. # RM-99106-S, Fisher, Thermo, QC) was used for staining, diluted 1:1000. Haematoxylin was used for counter staining[136].

2.8 Pathological Grading and Response

The modified Tumor Regression Grade (mTRG) [65] differentiates between two types of necrosis. The first is Usual Necrosis (UN), considered a negative prognostic factor and a form of tumor progression. The second is Infarct-like Necrosis (ILN), a positive prognostic factor and a form of response. UN is identified as small patches of necrosis mixed with nuclear debris and walled off by tumor cells, while ILN is seen as large pink confluent areas surrounded by a desmoplastic like ring. Two independent pathologists graded every lesion according to modified Tumor Regression Grade (mTRG). Grade 1, complete response, was defined as the absence of viable tumor. Grade 2, was defined by the presence of rare tumor cells and little to no UN (<10%). Grade 3, was defined when more than rare but less than predominant the sum of viable tumor cells and UN were present (10-49%). Grade 4, when the sum of viable tumor cells and UN is predominant (>50) but fibrosis is seen within or around tumor cell. Grade 5 was defined by the absence of fibrosis with predominant viable tumor cells.

2.9 Radiological Response

Radiological response to therapy was assessed according to Response Evaluation Criteria in Solid Tumors (RECIST 1.1) guidelines[137]. Baseline CT scans were performed before the start of chemotherapy and repeated in 8-12 weeks. Complete Response (CR) is defined by the

disappearance of all target lesions, Partial Response (PR) is defined by a 30% or more decrease in the sum of target lesions, Progressive Disease (PD) is defined by a 20% or more increase in the sum of the target lesions or the appearance on new lesions, and Stable Disease (SD) is when neither criteria for PR or PD is met. Target lesions are measured at their longest diameter in both baseline and follow-up CT scans. They must be of at least 10mm in the longest diameter on CT scan, a maximum of 5 lesions can be considered as target lesions per organ.

2.10 Matrix Application and Slide Preparation

1,5-Diaminonapthalene (1,5DAN) matrix is applied by sublimation[82]. A glassware apparatus connected to a cold trap that in turn is connected to a pump is used to create vacuum (Figure2.1). First, an oil bath in a spinning plate is heated to 160°C. Next a double compartment glass jar is placed above it, but not yet immersed. In the inner compartment of the glass jar cold water and ice (slush) is placed. The ITO coated glass slides with the specimen thawed on top are taped to the bottom of the inner compartment externally in a perpendicular fashion in regards to the vacuum spout. The matrix is placed inside the external jar and arranged opposite of the slides to facilitate sublimation. Once the apparatus is connected the pump is switched on. When sufficient vacuum is achieved and the oil is heated efficiently the double compartment jar is slowly immersed into the oil for 8-10 minutes, where the matrix will be sublimated.

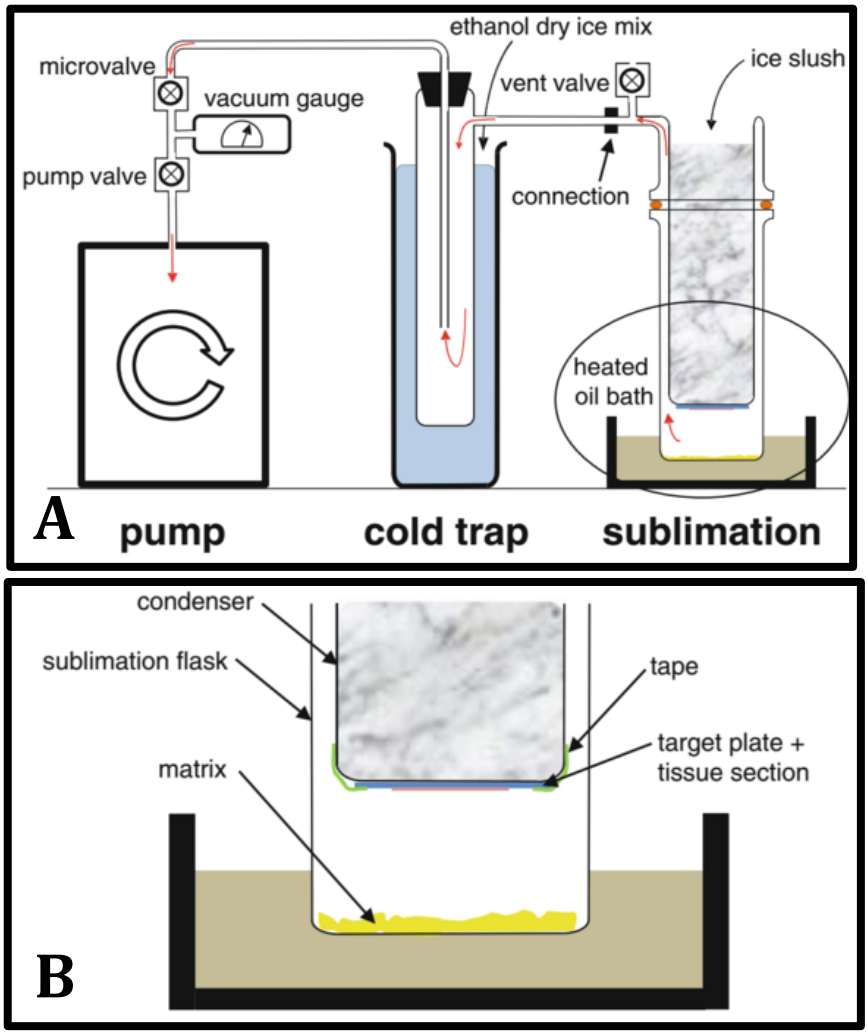

Figure 2.1 Scheme of Matrix Sublimation system. A Arrows indicate airflow. **B** Slide and matrix aliment.[138]

2.11 MALD-IMS Instrument Parameters

Bruker MALDI-TOF/TOF Ultraflextreme was used for IMS. Both positive and negative polarities were performed on serial sections, or in some cases on the same section with a 50µm shift in two directions. Mass resolution was set at 100 µm and 150 laser shores were summed per array position. Mass range was set at *m/z* 460-1200 for both ionization modes.

2.12 MALDI Tandem Mass Spectrometry

Tandem mass spectrometry or MS/MS is used to identify ions detected through fragmentation. To improve fragmentation, species detected in positive mode were acquired in Bruker Solarix 15 T FT-ICR using dried droplet spotting of 2,5-dihydroxyacetophenone doped with 100 mM Lithium Trifluoroacetate (LiTFA)[139] in addition to LIFT-TOF/TOF mode of the Ultraflexetreme. This preparation method is advantageous as lithium exhibits high affinity for phospholipids and facilities its ionization accordingly. Species detected in negative mode were directly identified through fragmentation with LIFT-TOF/TOF mode of the Ultraflexetreme.

3. RESULTS

3.1 Baseline Clinical Characteristics and Survival

A total of 52 lesions from 50 patients were included in this study. Table 3.1 shows patient characteristics for the entire study population (Training and Validation sets are displayed separately in Table 6.1 (appendix)). Twelve lesions sections were used for training while the rest was used for validation (n=40). The median age of diagnosis for the entire study cohort is 65 years of age with a range of 31 to 81 years. Male Patients constitute most of the study population (62%). The majority of primary disease lesions were in the colon, while 34% only were in the rectum. Most patients presented in a synchronous manner with the primary disease (63.4%). Over half of the patients had liver lesions in the right lobe (59.6%) while only 2 patients had bi-lobar disease. Furthermore, 46% have a single liver lesion while 17.3% have more than 4 lesions. Lesions averaged 3.7 cm in size at the longest diameter (range 0.3-10 cm). Most patients received neoadjuvant chemotherapy (67.3%), around half of which received Bevacizumab (54.2%). Three patients had complete response (CR), 13 patients had partial response (PR) and 15 had stable disease (SD), while only 4 patients had progressive disease (PD) two of which underwent PVE. Table 3.2 shows chemotherapy data for the entire study population as well as the correlation between radiological and pathological response to therapy (The two sets chemotherapy status is displayed separately in table 6.1).

At the last follow-up 8 mortalities were noted. All but one died from metastatic disease (two of which had brain metastasis). Estimated 1-year and 3-year OS were at 100%, and 82.6% respectively (26.5 months mean follow up duration). In addition, 27 (54%) patients had recurrence in the liver, 13 of those also had recurrence in the lungs, and another 4 patients recurred in the lungs without liver recurrence. Estimated 1-year, and 3-year DFS for liver

metastasis were at 49.9%, and 44.4% respectively (26.5 months mean follow up duration). Figure 3.1 shows patient survival for the entire cohort as well as for the training and validation sets separately.

Table 3.1 Patient Demographics.

Variable	No.(%)	Mean (SD)	Range
Age (years)*		63.1 (11.7)	31-81
Sex*			
Male	31 (62)		
Female	19 (38)		
Location of Primary Disease*			
Proper Colon	8 (16)		
Sigmoid Colon	15 (30)		
Rectum	17 (34)		
Unknown	10 (20)		
Stage of Primary Disease (TNM)*			
T (size)			
T1	1 (2)		
T2	2 (4)		
T3	27 (54)		
T4	8 (16)		
Unknown	12 (24)		
N (lymph node)			
N0	11 (22)		
N1	16 (32)		
N2	9 (18)		
Unknown	14 (28)		
Disease Free interval**			
Synchronous	33 (63.4)		
Metachronous	19 (36.5)		
Location of Liver Lesion**			
Right Lobe	31 (59.6)		
Left Lobe	19 (36.5)		
Bi-lobular	2 (3.8)		
No. of Lesions**		2.5 (2.1)	1-10
≤ 4	43 (82.6)		
> 4	9 (17.3)		
Size of Lesion (cm)**		3.7 (2.3)	0.3-10
≤ 5 cm	36 (69.2)		
> 5 cm	16 (30.7)		

*n=50 **n=52

Table 3.2 Chemotherapy Status and Response

Chemotherapy Status		n (%)	
Chemo-naïve*		17 (32.6)	
Chemo-treated*		35 (67.3)	
Chemotherapy alone**		16 (45.7)	
Bev+Chemotherapy**		19 (54.2)	
Radiological Response to Chemotherapy****	**Pathological Response to Chemotherapy***		
	Major Response n(%)	**Partial Response n(%)**	**Minor Response n(%)**
Complete Response	2 (66.6)	1(33.3)	0 (0)
Partial Response	6 (46.1)	2 (15.3)	5 (38.4)
Stable Disease	3 (20)	6 (40)	6 (40)
Progressive Disease	0 (0)	2 (50)	2 (50)

*n=52 **n=35 ***according to pathologist's mTRG[65] ****according to RECIST 1.1[137]

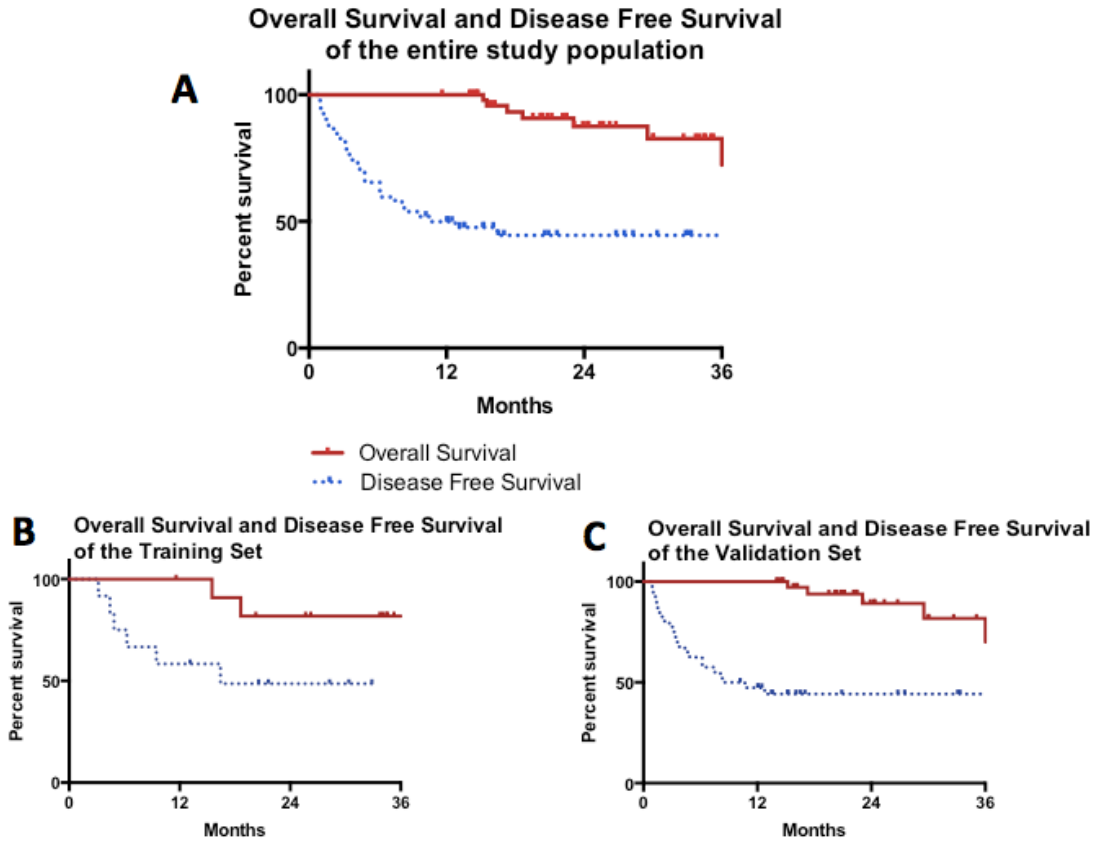

Figure 3.1 Overall Survival (OS) and Disease Free Survival (DFS). A Entire Study population survival proportions indicated in results. **B** Training Set: estimated 1-year and 3-year OS were observed at 100% and 81.8% respectively. Estimated 1-year and 3-year DFS were observed at 58.3% and 48.6% respectively. **C** Validation set: estimated 1-year and 3-year OS were observed at 100% and 81.6% respectively. Estimated 1-year and 3-year DFS were observed at 47.3% and 44.2% respectively.

3.2 Spectral Library Development:

To build a spectral library a semi-supervised histology-derived approach was done initially using a set of 12 samples. This was performed using clustering algorithms (k-means) instead of manually choosing ROI according to pathologist annotations, thus avoiding the introduction of non-relevant IMS pixels, which occurs with manual selection in microscopically heterogeneous samples such as tumor sections. Acquired spectra were clustered using spatially aware k-mean (k=7) algorithm for each sample (n=12), and correlated with a 5 stain histological panel (Apo F, PLTP, AB, Ki67 and H&E) as shown in figure 3.2. This proved adequate to distinguish molecular signatures pertaining to histological topographies as 6 of the 7 clusters were immediately correlated with histology (Figure3.3), and thus identified as topography specific lipid signatures. The 7th cluster correlated with background matrix and consequently excluded from further data mining. These identified topographies are normal liver, viable tumor, necrosis, fibrosis, inflammation and mucin. The associated lipid signatures are color coded as blue, red, purple, grey, green and white respectively throughout this dissertation (classification for the entire training set are displayed in Figure 6.1).

Each of the six lipid signatures is identified by a group of co-expressing ions. By comparing them in a one vs. all approach we were able to identify and select single lipid histology marker candidates while excluding markers that may express similarly in multiple signatures. Receiver operator characteristics (ROC) curves were calculated for all picked peaks, and area under the curve (auROC) was calculated to determine the most discriminant lipids for each signature. These lipids were subsequently fragmented to ascertain their identity (Figure 6.2). Table 3 indicates the most discriminant species' topographies, masses, auROCs, fold changes, identity, and characteristic MS/MS ions (combined Ion images are displayed in

figure 6.4). A tile plot of average peak intensity shows univariate comparisons of 14 top marker ions for the correlated topographies is shown in figure 3.4. Mucinous/empty histology was not included, as discriminant markers were 1.5-DAN matrix peaks. Another advantage of an automated means of data clustering is that it allows the comparison of signatures and therefore their designated histologies across the samples. By further dissecting the red signature we identified a lipid in the negative mode at *m/z* 835.54 with an expression intensity that correlates visually with ki67 IHC.

Table.3 Discriminate Ions

Topography	*m/z*	Identity	Fold change	auROC	MS/MS
Normal	NEG_738.5	**PE(16:0/20:4)**	3.161 ± 0.23	0.923	FA-1:255,FA-2:303,434(Etn),452(Etn)
	NEG_762.5	**PE(16:0/22:6)**	4.827 ± 0.45	0.940	FA-1:255,FA-2:327, 434(Etn),452(Etn), 506(Etn),524(Etn)
	NEG_885.56	**PI(18:0/20:4)**	3.227 ± 0.19	0.964	303, 283 (fatty acyl chains), 297 (Glycerophosphoinositol), 241 (Inositol phosphate ion)
	POS_758.57	**PC(16:0/18:2)**	2.71 ± 0.66	0.996	Li_fragmentation: 508(NL of 16:0), 484(NL of FA 18:2), 508(NL of 16:0), NL of 59, NL of 183 (PC headgroup)
Tumor	NEG_698.48	**PE(p-16:0/18:2)**	2.408 ± 0.42	0.878	FA-2: 279, 436 (Loss of sn2 acyl chain as ketene (RCH=C=O) from [M-H]-)
	NEG_700.51	**PE(p-16:0/18:1)**	2.151 ± 0.52	0.864	FA-2: 281, 436 (Loss of sn2 acyl chain as ketene (RCH=C=O) from [M-H]-)
	NEG_835.54	**PI(16:0/18:1)**	2.813 ± 0.63	0.885	281, 255 (fatty acyl chains), 297 (Glycerophosphoinositol), 241 (Inositol phosphate ion), 673(NL of inositol)
	POS_706.55	**PC(14:0/16:0)**	2.835 ± 0.51	0.829	184(PC headgroup), ~0.7 ppm error
	POS_732.55	**PC(16:0/16:1)**	5.355 ± 1.29	0.921	Li_fragmentation: 480(NL of 16:1), 482(NL of 16:0), NL of 59, NL of 183 (PC headgroup)
Inflammation	NEG_722.49	**PE(p-16:0/20:4)**	3.749 ± 0.62	0.935	436(Loss of sn2 acyl chain as ketene (RCH=C=O) from [M-H]-), 303(FA chain)
	NEG_750.53	**PE(p-18:0/20:4)**	3.744 ± 0.66	0.845	464 (Loss sn2 acyl chain as ketene (RCH=C=O) from [M-H]-), 303(FA)
	POS_734.57	**PC(16:0/16:0)**	3.673 ± 0.72	0.942	Li_fragmentation: 478(NL of 16:0), NL of 59, NL of 183 (PC headgroup)
Fibrosis	POS_782.55	**PC(18:2/18:2)**	1.5 ± 0.61	0.780	184(phophotidylcholine headgroup)
Necrosis	POS_703.57	**SM(d18:1/16:0)**	5.62 ± 0.66	0.902	Li_fragmentation: 280(sn-2 loss), NL of 59, NL of 183 (PC headgroup)

Etn = ethanolamine. NL = neutral loss. FA = fatty acid. PC = phosphotidylcholine. PE=phosphoethanolamine. SM = Sphingomyelin. p-16:0/p-18:0 = plasmenyl lipid. Cer = Ceramide. PI = phosphoinositol.

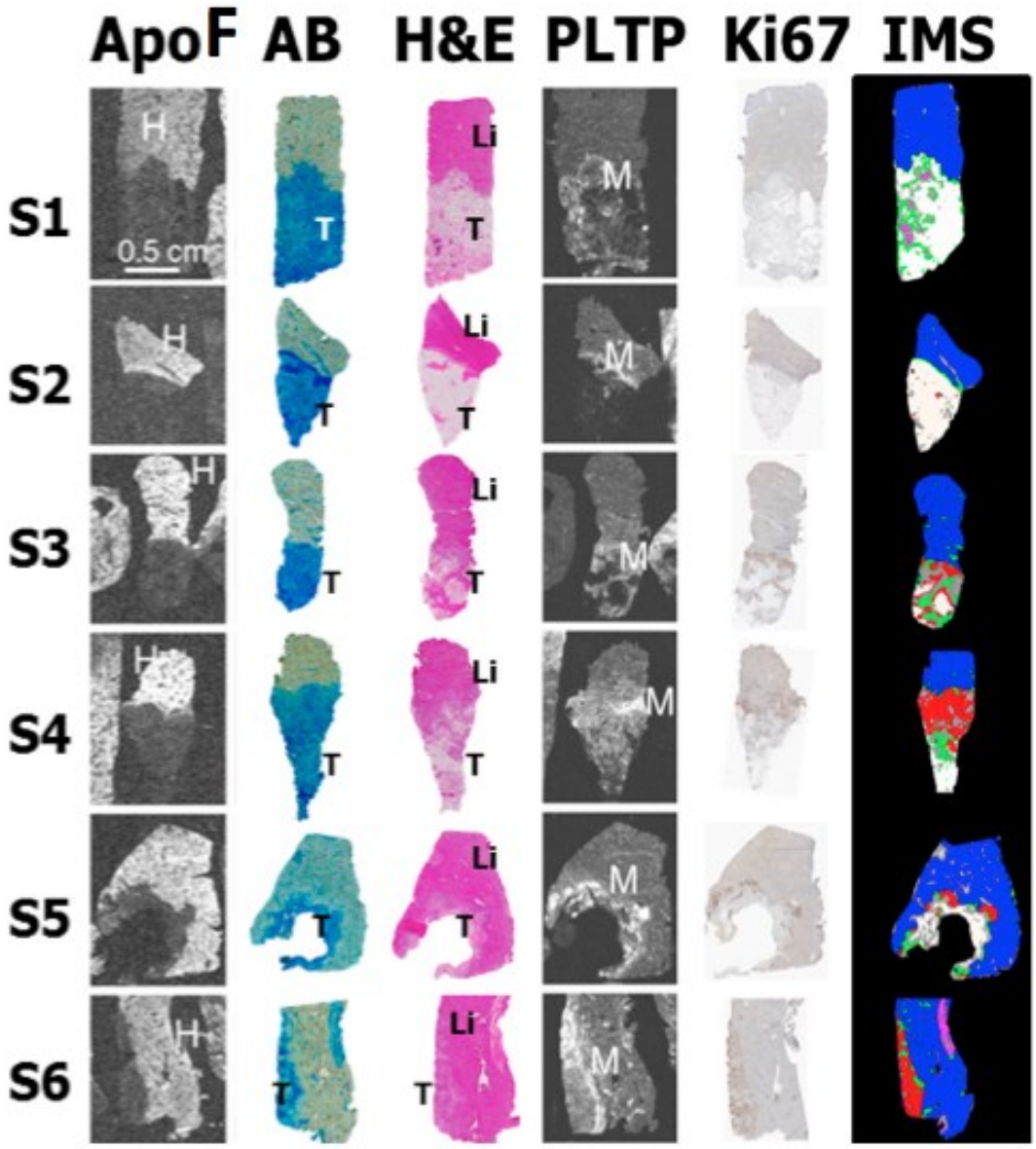

Figure 3.2 Histological 5-stain Panel. A representative subset of the training samples. (ApoF) apolipoproteIn F (AB) alcian blue, (H&E) hematoxylin and eosin, (PLTP) phospolipid transfer protein, (Ki67) proliferation index

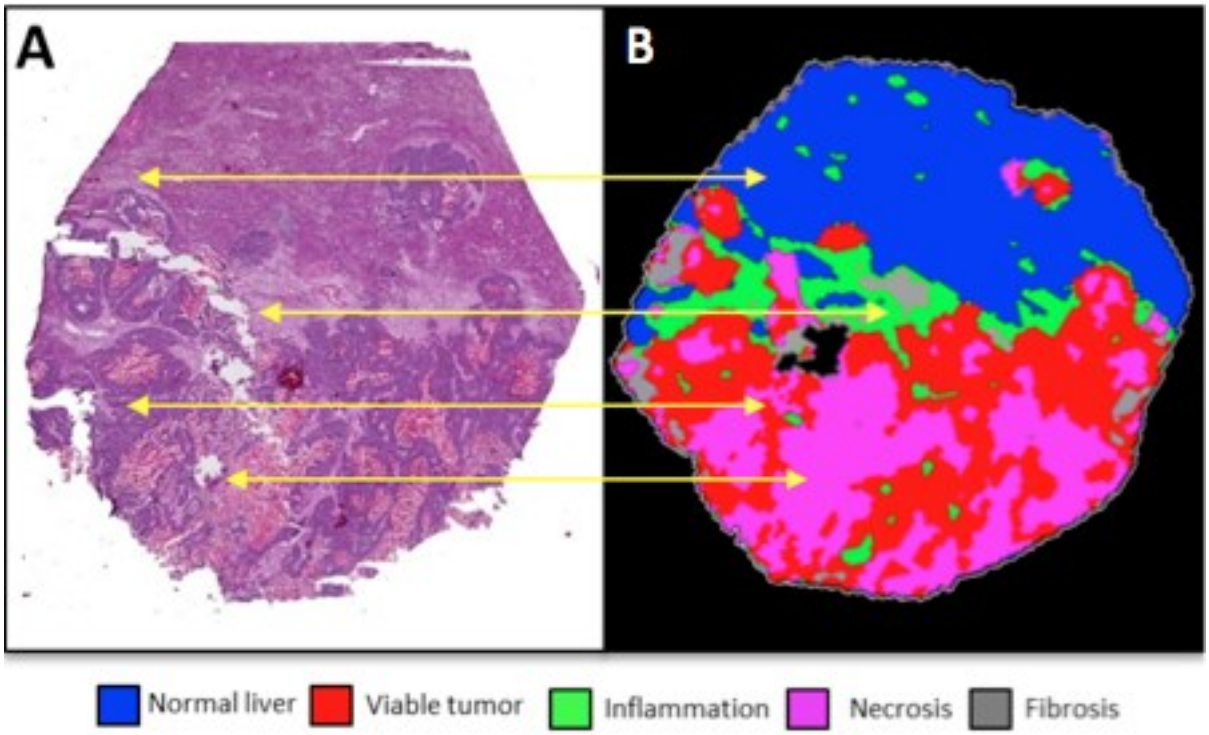

Figure 3.3 Histological Correlation. A H&E scan of serial section. **B** Lipid signatures (5 of the identified 6 are showing). Yellow arrows draw direct spatial correlation between lipid signatures and their designated histologies.

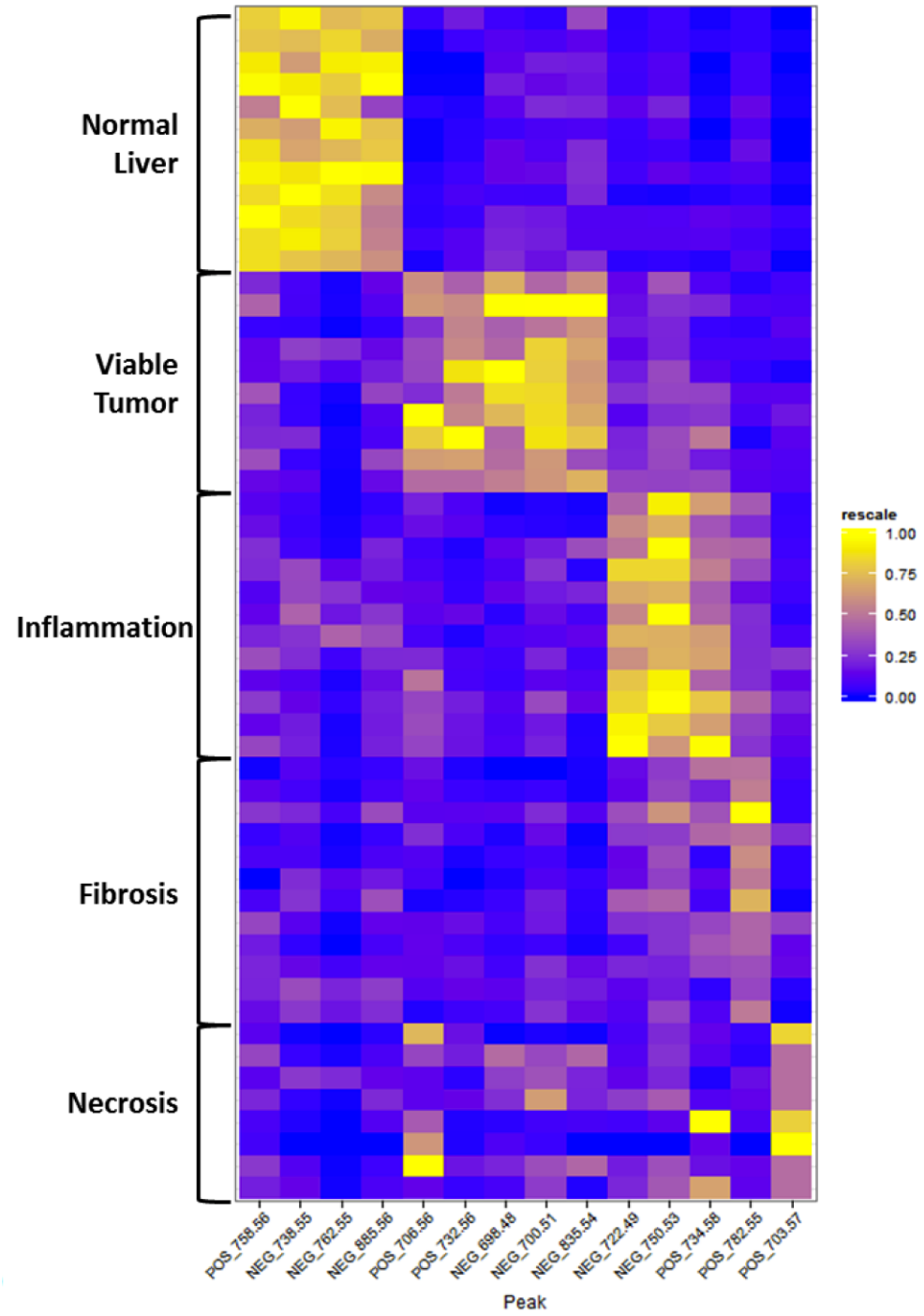

Figure 3.4 Histology Lipid Markers. A tile plot of average peak intensity shows univariate comparisons of 14 top marker ions and their co-expression.

3.3 Validation of Lipid Signatures

We used the spectral library developed by collation of the identified lipid signatures of the training-set to classify the topography of 40 additional samples. According to their lipid profiles and coordinates each IMS pixel of the validation set samples was classified to a single lipid signature or another using Partial Least Squares – Discriminant Analysis (PLS-DA). The IMS predictions of topography were validated retrospectively for the entire validation set (n=40) by a pathologist using high resolution H&E scans. Figure 3.5 illustrates three of the samples and their validation score. The rest of the validation's set histological correlations are shown in Figure 6.3. Very strong correlations were observed between predicted topography and gross morphology.

Validation was done by scoring each lipid signature in every lesion from 0 to 5. A lipid signature was only scored '0' if its correlated histology was not present in the H&E section while it was on the IMS predications or vice-versa. A score of 1 indicated that $1/5^{th}$ of the histology is matching and a score of 5 indicated a complete correlation. The green and grey signatures were scored as one signature as their designated histologies (inflammation and fibrosis respectively) were difficult to distinguish between based solely on H&E without further histopathological staining. The Blue (adjacent normal), Red (tumor), Purple (necrosis), Grey/Green (fibrosis/inflammation) and White (loose tissue/mucin) signatures scored an average of 5, 4.9, 4.5, 4.9, and 4.7 respectively indicating a very high level of correlation between the IMS prediction of all histologies in this cohort of lesions. Most H&E scans were of a direct serial section of that used for IMS, however when that was not the case (n=4) special consideration was taken by the pathologist and correlation remained strong.

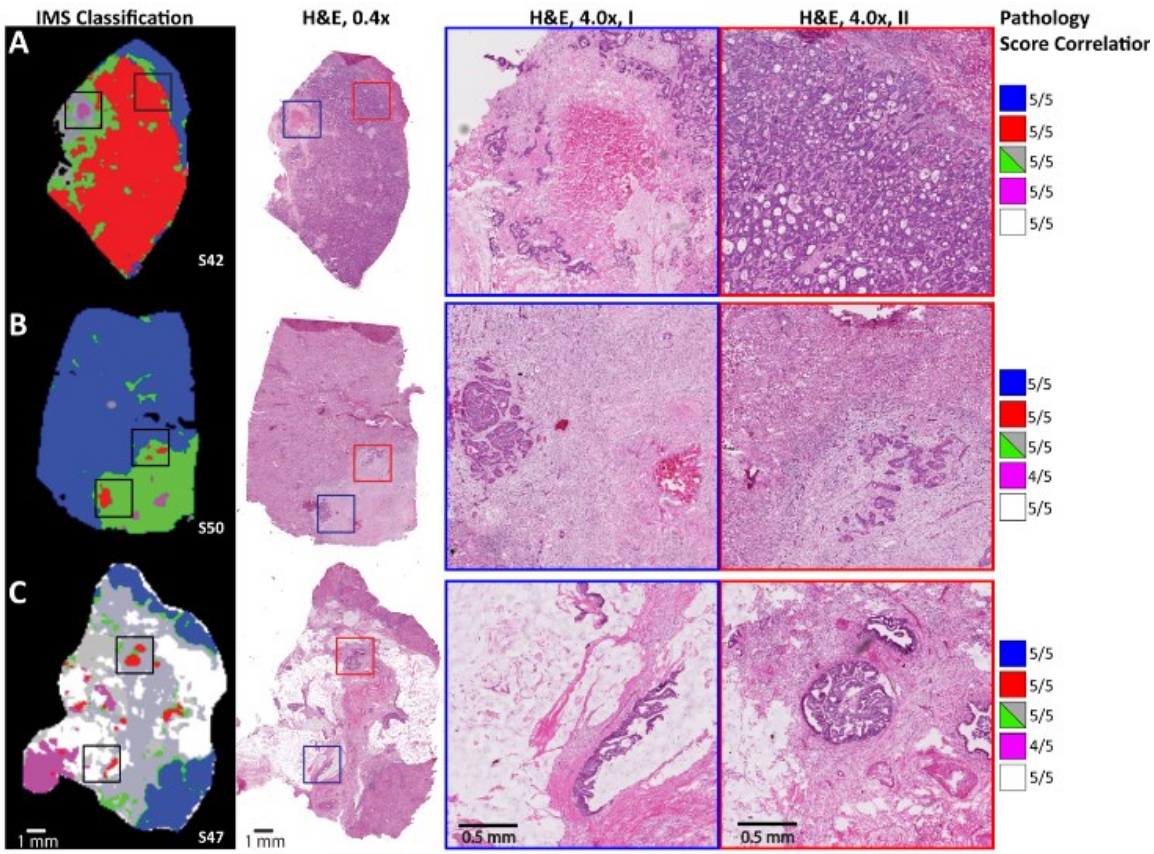

Figure 3.5 Validation process. Three representative samples. **A** Tumor predominant sample reflected in the red lipid signature. High resolution H&E scan shows small amount of necrosis was picked up. **B** Sample with 2 small foci of viable tumor accurately detected in IMS lipid signatures. **C** Histologically heterogeneous sample.

3.4 Purple Signature Mining

The Modified Tumor Regression Grade (mTRG) as described by *Chang et al*. differentiates between two type of necrosis, Infarct-like Necrosis (ILN) and Usual Necrosis (UN) namely. Thus, further mining of the Purple signature (correlating with necrotic topography) was deemed necessary to generate automated mTRG using our lipid signatures. This was done by manual mining of top ion hits of the purple signature and comparing their ion images to histopathology. Once ions were selected as candidate markers for each type of necrosis

MS/MS was performed to ascertain their identity (Table.4). We were able to differentiate these two types of necrosis using single lipid ions in both polarities. In positive mode (Figure3.6) we identified a sphingomyelin species to be abundant in ILN at *m/z* 703.57 (SM (d18:1/16:0)) and two series of plasmalogens abundant at UN at *m/z* 746.57 (PC (p-16:0/18:0)) and 744.57 (PC (p-16:0/18:1)). In negative mode we identified two ceramide species; one to be abundant in UN at *m/z* 536.50 (Cer (d18:1/16:0) and another abundant in ILN at *m/z* 616.47 (Cer-1-P(d18:1/16:0)).

Table.4 Necrosis Specific Discriminate Ions

Topography	m/z	Identity	Fold change	auROC	MS/MS
Infarct-like Necrosis	POS_703.57	**SM(d18:1/16:0)**	5.62 ± 0.66	0.902	Li_fragmentation: 280(sn-2 loss), NL of 59, NL of 183 (PC headgroup)
	NEG_616.47	**Cer-1-P(d18:1/16:0)**	4.83 ± 1.12	0.880	96(phosphate group),78(phosphate-H_2O)
Usual Necrosis	POS_742.57	**PC(p-16:0/18:2)**	2.20 ± 0.43	0.823	Li_fragmentation: NL of 189 (PC headgroup),279(NL of 189 + NL of non-plasmenyl FA)
	POS_744.59	**PC(p-16:0/18:1)**	5.16 ± 1.14	0.911	Li_fragmentation: NL of 189 (PC headgroup),279(NL of 189 + NL of non-plasmenyl FA)
	POS_746.59	**PC(p-16:0/18:0)**	5.56 ± 0.78	0.912	Li_fragmentation: NL of 189 (PC headgroup),279(NL of 189 + NL of non-plasmenyl FA)
	POS_768.57	**PC(p-18:0/18:3)**	5.02 ± 0.98	0.902	Li_fragmentation: NL of 189 (PC headgroup),307(NL of 189 + NL of non-plasmenyl FA)
	POS_770.59	**PC(p-18:0/18:2)**	3.94 ± 0.74	0.872	Li_fragmentation: NL of 189 (PC headgroup),307(NL of 189 + NL of non-plasmenyl FA)
	POS_772.59	**PC(p-18:0/18:1)**	3.54 ± 0.88	0.854	Li_fragmentation: NL of 189 (PC headgroup),307(NL of 189 + NL of non-plasmenyl FA)
	NEG_536.50	**C16 Cer(d18:1/16:0)**	4.83 ± 1.19	0.945	506(NL of H_2CO), 504(NL of H_2-H_2CO), 488(NL of H_2O-H_2CO), 296(side chain loss), 254(FA loss)

NL = neutral loss. FA = fatty acid. PC = phosphotidylcholine.. SM = Sphingomyelin. p-16:0/p-18:0 = plasmenyl lipid. Cer = Ceramide.

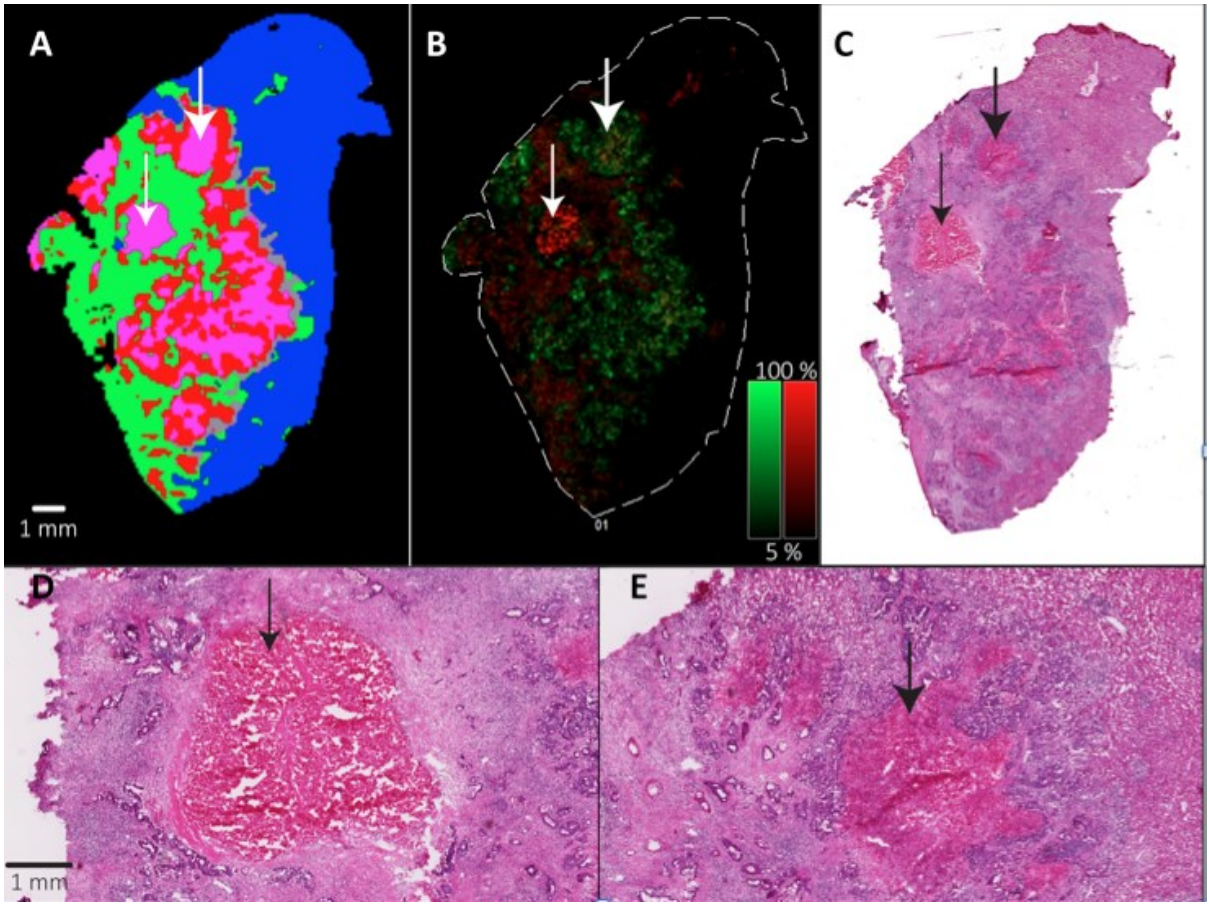

Figure 3.6 Purple Signature Mining. A Lipid signatures. White arrow points two foci of necrosis of different types. **B** By manual mining of the signature we identified single lipid markers for each by correlation with H&E **(C)**. **D** High magnification of ILN on H&E. **E** High magnification of UN on H&E.

3.5 Molecular Based mTRG

To evaluate the robustness of the classifications -based on lipid signatures including those distinguishing UN and ILN- and its clinical application we generated an automated objective mTRG score established by the IMS data. Based on published mTRG scoring guidelines[65] we developed an algorithm applicable to IMS lipid signatures. The algorithm applies the following parameters; grade 1 was defined by the absence of the red signature (identified as viable tumor), grade 2 was defined by <7% of the sum of the red signature and UN signature

in relation to other signatures (7% was chosen as a cut-off as opposed to pathologist eye-ball estimate of 10% by correlating pathologist estimates to IMS quantifications), grade 3 by ≥ 7% but <50% of the sum of the red signature and UN signature in relation to other segments, grade 4 by ≥ 50% of the sum of the red signature and UN signature in relation to other signatures and grade 5 by ≥ 50% of the sum of the red signature and UN signature in relation to other signatures and the absence of the grey signature (identified as fibrosis). To validate our method we correlated the scores for all the lesions (n=52) with scores of two independent blinded pathologists. Inter-pathologist correlation was observed at r=0.7361 shown in Table 5 ($p<0.0001$). The IMS generated scores correlated with both pathologists (r=0.8121 and r=0.6227, for pathologist 1 and 2, respectively, ($p<0.0001$)). It is noteworthy to mention that a few lesions were deemed too small for assessment by Pathologist 2, further details are in table 6.2.

To further drive this correlation and observe its clinical relevance we plotted the mTRG grades from the two pathologist and lipid signatures (IMS mTRG) to overall survival (OS) and disease free survival (DFS) as seen in Figure 3.7. Patients who received chemotherapy were stratified into three response groups according to theirs scores (major response: grades 1 and 2, partial response: grade 3, and minor response: grades 4 and 5)[62]. Three-year OS and DFS were calculated for each response group (Pathologist 1, Pathologist 2 and IMS mTRG) and homogenous trends were observed. Interestingly the major response group selected by IMS has significantly better DFS than those selected to be major response by either pathologists. This suggests that IMS increased sensitivity allows for better patient stratification as illustrated in Figure 3.7B.

Table.5 IMS Generated mTRG Correlations

	Pathologist 1	Pathologist 2	MALDI
Pathologist 1		0.7361	0.8121
Pathologist 2	0.7361		0.6227
MALDI	0.8121	0.6227	
Average	0.7741	0.6794	0.7174

P<0.0001 for all correlations.

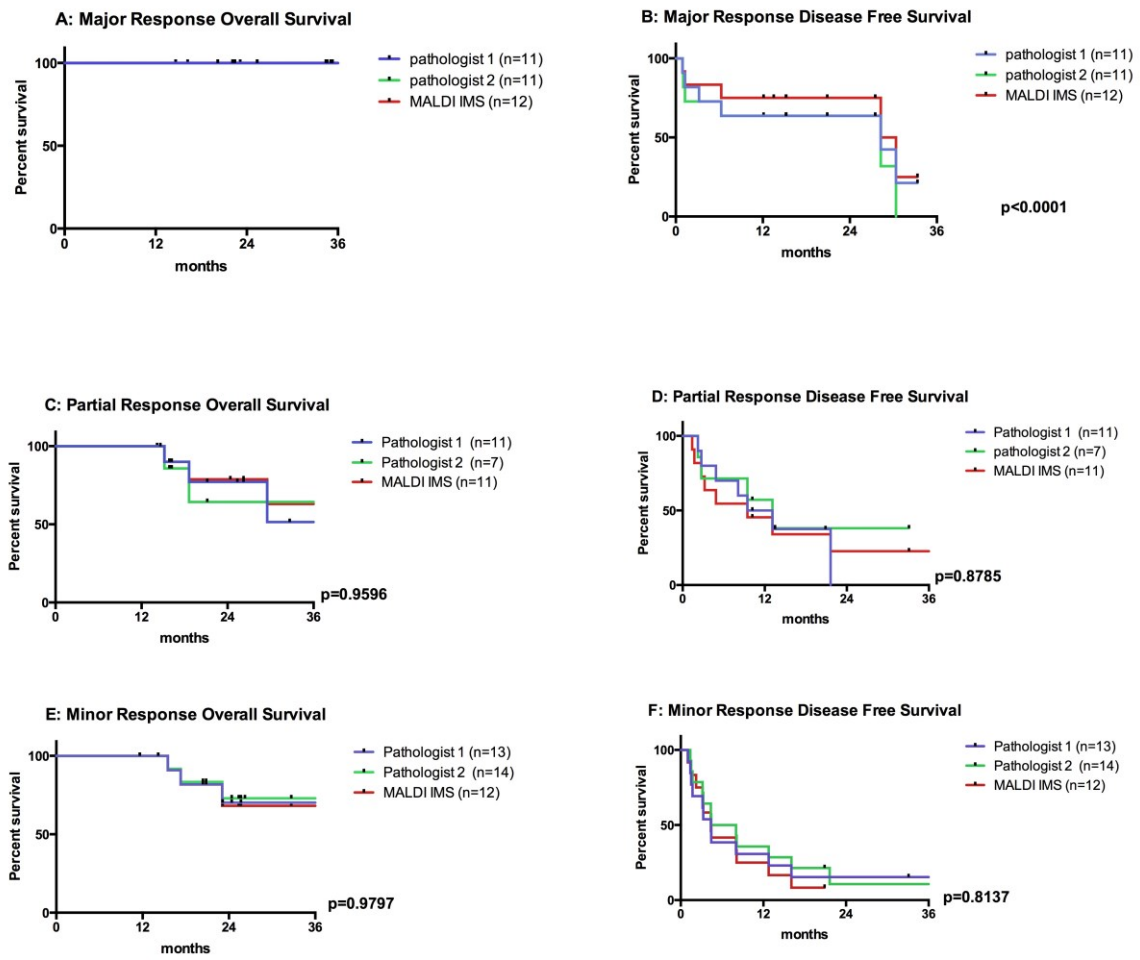

Figure 3.7: Kaplan–Meier Survival Analysis For The Three Response Groups stratified according to pathological grading as observed by two independent pathologists and by MALDI IMS. The p value of the log-rank test is shown. **A:** Overall survival (OS) curve for major response group showing 100% OS at 12 and 36 in all three observation groups. No events in this patient group. All data censored. **B:** Disease Free Survival (DFS) curve for major response groups showing 63.6% DFS for the pathologist 1 and pathologist 2 and 75% DFS for MALDI IMS at 12 months and 21.7%, 0% and 38% DFS for Pathologist 1, Pathologist 2 and MALDI IMS at 36 months respectively.**C:** OS curve for partial response group showing 100% OS at 12 months for all three observation groups and 51.4%, 64.2% and 63% OS at 36 months for pathologist 1, pathologist 2 and MALDI IMS respectively. **D:** DFS curve for partial response groups showing 54.5%, 57.1% and 45.4% DFS at 12 and 0%, 38% and 22.7% at 36 months for the pathologist 1, pathologist 2 and MALDI IMS respectively. **E:** OS curve for minor response group showing 100% OS at 12 months for all three observation groups and 70.1%, 72.9% and 68.1% OS at 36 months for pathologist 1, pathologist 2 and MALDI IMS respectively. **F:** DFS curve for minor response group showing 30.7%, 35.7% and 25% DFS at 12 months and 15.3%, 10.7% and 8.3% DFS at 36 months for pathologist 1, pathologist 2 and MALDI IMS respectively.

4. DISCUSSION

We were able to generate an automated objective histologically quantitative mTRG using MALDI IMS based lipid signatures. This allowed us to stratify patients into response groups and accurately predict their outcome (overall survival and disease free survival), thus providing pathologists and clinicians with a valuable objective tool to prognosticate patients and further drive treatment options and decisions. Unlike previous works in the field that relied on pathologist annotation to select ROI in a histology driven approach, we scanned the entire tissue section using MALDI IMS and included the entirety of the data in our analysis, thus alleviating possible error that might occur during ROIs selection and increasing statistical power of inter-sample comparison. A possible concern in including the whole resection sample in the analysis is that it often takes into consideration areas of inflammation adjacent to the tumor foci but not within it, therefore overestimating inflammation. However, despite this slight overestimation, grades remained the same throughout the cohort in the fully automated grading (no manual ROI selection), when compared to grades where ROI (entire lesion area, not histology specific ROI) were selected ($r=0.98$ $p<0.001$). In addition, previous studies aimed to distinguish cancer lesions from adjacent normal and distant normal tissue with a single or a few lipid intensities, while our approach allowed us to explore the TME at a deeper level. This is significant because cancer lesions are composed of multiple tissue types, and the progression and regression of these lesions is a dynamic process with composition changes reflecting the status of the lesion.

Classifications based on IMS data will be key in clinical analysis. It will not be practical for a routine clinical pathology lab to examine IMS data ion by ion. Furthermore, many molecules detected by IMS are generic and will be expressed by several types of cells, with changes in their relative abundance distinguishing histologies and prognoses. Although the discovery

phase and classifications will require the full MALDI setting, the initial cost of introducing MALDI IMS into the clinical setting can be reduced by opting for a counter-top device that is already utilized in many microbiology clinical laboratories. Furthermore, aside from objectivity, using this method, a synoptic pathology report can be automated and produced within two hours from start to finish.

In addition, from a research standpoint, correlating IMS raw data with clinical variables is not feasible due to the limited number of observations in typical clinical studies compared to the huge set of data generated by this type of analysis. Our training and validation sets were selected according to procurement dates to avoid selection bias. Although the two groups of patients are clinically comparable this coincidently resulted in under representation of ILN in training set lesions, which necessitated further mining of the purple cluster. This could be avoided by hand selecting histologically representative sample for training, leading to upfront separate clustering of the two types of necrosis. Another possible limitation of our study was the subjectivity of the validation process. A technical objective validation can be done by randomly assigning samples into multiple training sets and comparing their classification in a single validation set. Nonetheless for the purpose of clinical applications pathologist's validation will remain necessary despite its subjective nature. Lastly, the small study sample and short follow up duration (median 26 months) limit the generalization of our findings. A longer multi institute study with a larger cohort is needed for validation.

MALDI IMS plays a role beyond pathological grading as a valuable biomarker candidate discovery tool. Within the necrosis areas we examined, we identified C16 ceramide and C16 ceramide-1-phosphate (C1P) associated with UN and ILN, respectively. C16 ceramide has been described as having tumor suppressor activity as it is thought to be anti-proliferative and

pro-apoptotic, while in contrast C1P has pro-survival anti-apoptotic activity, making these lipids attractive biomarker candidates[140,141]. It has been reported that high levels of C1P - which stimulates cell division and inhibits apoptosis- is toxic and can kill cells[142]. The two ceramide markers correlation within the two distinct and differentially prognostic necrosis areas could potentially lead to a novel target. Alongside the ceramides, plasmalogens were identified in the necrosis areas. Although found ubiquitously in human cells, they have not been previously described in cancer or necrosis processes, unlike other ether lipids. In addition, they have been reported to be lower in abundance in liver tissue compared to other organs[142,143]. Interestingly, within our data set we identified PE (phosphoethanolamine) plasmalogens to be associated with both tumor areas and areas of inflammation, whereas PC plasmalogens are exclusively abundant in areas of UN. Current research indicates PE plasmalogens as the precursor to PC plasmalogens as no plasmenylcholine desaturase enzyme has been described. Compared to UN, we find minimal PC plasmalogen signal in surrounding liver tissue. The function of these lipids in the specific histologies opens further areas of research.

IMS and MALDI offer a unique exploration of spatial information. Resection margins largely affect patient outcome and are regarded as an independent prognostic factor. Considering that MALDI IMS has a higher sensitivity in detecting viable tumor, as proven by the superior outcome of patients regarded as Major Response group by IMS signatures, its employment in margins assessment could be greatly beneficial to clinical practice. Furthermore, with a suitable spectral library it can generate a detailed automated pathological grading in as little as 30 min – 2 hours depending on sample size. In addition, by building a larger more heterogeneous spectral library with various types of cancers, MALDI IMS could be used for diagnostic purposes in differentiating cancer type based on lipid profiles. Not only can the

tissue section be used for downstream staining after acquiring data, but also the IMS data can be mined at any point of time with reproducible methods, and correlated with different tissue markers. It can also be used to replace a number of histological stains and antibodies, which will lead to lower overall costs. For example, in our set of data we have identified a mucin signature which can replace AB staining, which allows for an actual quantification and overcomes staining and IHC methods limitations[144].

Advances in MS have facilitated lipidomic applications in biomarker discovery. Liquid chromatography (LC/MS) is already being widely used for discovering and identifying lipid biomarkers in blood samples[145]. Our study demonstrates IMS applications in CRCLM histopathology and biomarker discovery using lipidomics. We have uncovered a novel set of markers (ceramides and plasmalogens) that can be further investigated to better understand the underlying pathology and be used as possible novel drug targets.

5. REFERENCES

1. Ferlay J, S.I., Ervik M, Dikshit R, Eser S, Mathers C, Rebelo M, Parkin DM, Forman D, Bray, F. GLOBOCAN 2012 v1.0, Cancer Incidence and Mortality Worldwide: IARC CancerBase No. 11 [Internet].

Lyon, France: International Agency for Research on Cancer. (2013).

2. Howlader N, N.A., Krapcho M, Garshell J, Miller D, Altekruse SF, Kosary CL, Yu M, Ruhl J, Tatalovich Z,Mariotto A, Lewis DR, Chen HS, Feuer EJ, Cronin KA SEER Cancer Statistics Review, 1975-2012, National Cancer Institute. Bethesda, MD, http://seer.cancer.gov/csr/1975_2012/,. (April 2015.).
3. American Cancer Society, Cancer Facts & Figures 2015.
4. Siegel, R., Desantis, C. & Jemal, A. Colorectal cancer statistics, 2014. *CA: a cancer journal for clinicians* **64**, 104-117 (2014).
5. Kemeny, N. Management of liver metastases from colorectal cancer. *Oncology* **20**, 1161-1176, 1179; discussion 1179-1180, 1185-1166 (2006).
6. Robertson, D.J., Stukel, T.A., Gottlieb, D.J., Sutherland, J.M. & Fisher, E.S. Survival after hepatic resection of colorectal cancer metastases: a national experience. *Cancer* **115**, 752-759 (2009).
7. Spolverato, G., Ejaz, A., Azad, N. & Pawlik, T.M. Surgery for colorectal liver metastases: The evolution of determining prognosis. *World journal of gastrointestinal oncology* **5**, 207-221 (2013).
8. Wei, A.C.*, et al.* Survival after hepatic resection for colorectal metastases: a 10-year experience. *Annals of surgical oncology* **13**, 668-676 (2006).
9. Pawlik, T.M.*, et al.* Effect of surgical margin status on survival and site of recurrence after hepatic resection for colorectal metastases. *Annals of surgery* **241**, 715-722, discussion 722-714 (2005).
10. Charnsangavej, C.*, et al.* Selection of patients for resection of hepatic colorectal metastases: expert consensus statement. *Annals of surgical oncology* **13**, 1261-1268 (2006).
11. Adam, R. Chemotherapy and surgery: new perspectives on the treatment of unresectable liver metastases. *Annals of oncology : official journal of the European Society for Medical Oncology / ESMO* **14 Suppl 2**, ii13-16 (2003).
12. Elias, D.*, et al.* Extrahepatic disease does not contraindicate hepatectomy for colorectal liver metastases. *The British journal of surgery* **90**, 567-574 (2003).
13. de Haas, R.J.*, et al.* R1 resection by necessity for colorectal liver metastases: is it still a contraindication to surgery? *Annals of surgery* **248**, 626-637 (2008).
14. Dhir, M., Lyden, E.R., Smith, L.M. & Are, C. Influence of margins on disease free survival following hepatic resection for colorectal metastasis: a meta-analysis. *Indian journal of surgical oncology* **3**, 321-329 (2012).
15. Yigitler, C.*, et al.* The small remnant liver after major liver resection: how common and how relevant? *Liver transplantation : official publication of the American Association for the Study of Liver Diseases and the International Liver Transplantation Society* **9**, S18-25 (2003).
16. Kim, H.J.*, et al.* Comparison of remnant to total functional liver volume ratio and remnant to standard liver volume ratio as a predictor of postoperative liver function after liver resection. *Korean journal of hepato-biliary-pancreatic surgery* **17**, 143-151 (2013).

17. Guglielmi, A., Ruzzenente, A., Conci, S., Valdegamberi, A. & Iacono, C. How much remnant is enough in liver resection? *Digestive surgery* **29**, 6-17 (2012).
18. Lin, X.J., Yang, J., Chen, X.B., Zhang, M. & Xu, M.Q. The critical value of remnant liver volume-to-body weight ratio to estimate posthepatectomy liver failure in cirrhotic patients. *The Journal of surgical research* **188**, 489-495 (2014).
19. Wicherts, D.A.*, et al.* Impact of portal vein embolization on long-term survival of patients with primarily unresectable colorectal liver metastases. *The British journal of surgery* **97**, 240-250 (2010).
20. Makuuchi, M.*, et al.* Preoperative portal embolization to increase safety of major hepatectomy for hilar bile duct carcinoma: a preliminary report. *Surgery* **107**, 521-527 (1990).
21. Hoekstra, L.T.*, et al.* Tumor progression after preoperative portal vein embolization. *Annals of surgery* **256**, 812-817; discussion 817-818 (2012).
22. Abdalla, E.K.*, et al.* Improving resectability of hepatic colorectal metastases: expert consensus statement. *Annals of surgical oncology* **13**, 1271-1280 (2006).
23. Adam, R.*, et al.* Rescue surgery for unresectable colorectal liver metastases downstaged by chemotherapy: a model to predict long-term survival. *Annals of surgery* **240**, 644-657; discussion 657-648 (2004).
24. Adam, R.*, et al.* Managing synchronous liver metastases from colorectal cancer: A multidisciplinary international consensus. *Cancer treatment reviews* **41**, 729-741 (2015).
25. Nordlinger, B.*, et al.* Perioperative chemotherapy with FOLFOX4 and surgery versus surgery alone for resectable liver metastases from colorectal cancer (EORTC Intergroup trial 40983): a randomised controlled trial. *Lancet* **371**, 1007-1016 (2008).
26. Chemotherapy of metastatic colorectal cancer. *Prescrire international* **19**, 219-224 (2010).
27. Chemotherapy of metastatic colorectal cancer: fluorouracil plus folinic acid and irinotecan or oxaliplatin. *Prescrire international* **14**, 230-233 (2005).
28. Saltz, L.B.*, et al.* Irinotecan plus fluorouracil/leucovorin for metastatic colorectal cancer: a new survival standard. *The oncologist* **6**, 81-91 (2001).
29. Goldberg, R.M.*, et al.* Randomized controlled trial of reduced-dose bolus fluorouracil plus leucovorin and irinotecan or infused fluorouracil plus leucovorin and oxaliplatin in patients with previously untreated metastatic colorectal cancer: a North American Intergroup Trial. *Journal of clinical oncology : official journal of the American Society of Clinical Oncology* **24**, 3347-3353 (2006).
30. Garcia-Alfonso, P.*, et al.* Neoadjuvant and conversion treatment of patients with colorectal liver metastasis: the potential role of bevacizumab and other antiangiogenic agents. *Targeted oncology* **10**, 453-465 (2015).
31. Gruenberger, T.*, et al.* Bevacizumab plus mFOLFOX-6 or FOLFOXIRI in patients with initially unresectable liver metastases from colorectal cancer: the OLIVIA multinational randomised phase II trial. *Annals of oncology : official journal of the European Society for Medical Oncology / ESMO* **26**, 702-708 (2015).
32. Masi, G.*, et al.* Bevacizumab with FOLFOXIRI (irinotecan, oxaliplatin, fluorouracil, and folinate) as first-line treatment for metastatic colorectal cancer: a phase 2 trial. *The Lancet. Oncology* **11**, 845-852 (2010).

33. Hu, W., Xu, W.S., Liao, X.F. & He, H.J. Bevacizumab in combination with first-line chemotherapy in patients with metastatic colorectal cancer: a meta-analysis. *Minerva chirurgica* **70**, 451-458 (2015).
34. Nasti, G.*, et al.* Neoadjuvant FOLFIRI+bevacizumab in patients with resectable liver metastases from colorectal cancer: a phase 2 trial. *British journal of cancer* **108**, 1566-1570 (2013).
35. Li, X.X., Liang, L., Huang, L.Y. & Cai, S.J. Standard chemotherapy with cetuximab for treatment of colorectal cancer. *World journal of gastroenterology* **21**, 7022-7035 (2015).
36. Zhang, L., Ma, L. & Zhou, Q. Overall and KRAS-specific results of combined cetuximab treatment and chemotherapy for metastatic colorectal cancer: a meta-analysis. *International journal of colorectal disease* **26**, 1025-1033 (2011).
37. Niekel, M.C., Bipat, S. & Stoker, J. Diagnostic imaging of colorectal liver metastases with CT, MR imaging, FDG PET, and/or FDG PET/CT: a meta-analysis of prospective studies including patients who have not previously undergone treatment. *Radiology* **257**, 674-684 (2010).
38. van Kessel, C.S.*, et al.* Preoperative imaging of colorectal liver metastases after neoadjuvant chemotherapy: a meta-analysis. *Annals of surgical oncology* **19**, 2805-2813 (2012).
39. Therasse, P.*, et al.* New guidelines to evaluate the response to treatment in solid tumors. European Organization for Research and Treatment of Cancer, National Cancer Institute of the United States, National Cancer Institute of Canada. *Journal of the National Cancer Institute* **92**, 205-216 (2000).
40. Lastoria, S.*, et al.* Early PET/CT scan is more effective than RECIST in predicting outcome of patients with liver metastases from colorectal cancer treated with preoperative chemotherapy plus bevacizumab. *Journal of nuclear medicine : official publication, Society of Nuclear Medicine* **54**, 2062-2069 (2013).
41. Lencioni, R. & Llovet, J.M. Modified RECIST (mRECIST) assessment for hepatocellular carcinoma. *Seminars in liver disease* **30**, 52-60 (2010).
42. Edeline, J.*, et al.* Comparison of tumor response by Response Evaluation Criteria in Solid Tumors (RECIST) and modified RECIST in patients treated with sorafenib for hepatocellular carcinoma. *Cancer* **118**, 147-156 (2012).
43. Egger, M.E.*, et al.* Assessment of chemotherapy response in colorectal liver metastases in patients undergoing hepatic resection and the correlation to pathologic residual viable tumor. *Journal of the American College of Surgeons* **216**, 845-856; discussion 856-847 (2013).
44. Chun, Y.S.*, et al.* Association of computed tomography morphologic criteria with pathologic response and survival in patients treated with bevacizumab for colorectal liver metastases. *Jama* **302**, 2338-2344 (2009).
45. Nathan, H.*, et al.* Conditional survival after surgical resection of colorectal liver metastasis: an international multi-institutional analysis of 949 patients. *Journal of the American College of Surgeons* **210**, 755-764, 764-756 (2010).
46. Fong, Y., Fortner, J., Sun, R.L., Brennan, M.F. & Blumgart, L.H. Clinical score for predicting recurrence after hepatic resection for metastatic colorectal cancer: analysis of 1001 consecutive cases. *Annals of surgery* **230**, 309-318; discussion 318-321 (1999).
47. Moertel, C.G.*, et al.* An evaluation of the carcinoembryonic antigen (CEA) test for monitoring patients with resected colon cancer. *Jama* **270**, 943-947 (1993).

48. Nordlinger, B.*, et al.* Surgical resection of colorectal carcinoma metastases to the liver. A prognostic scoring system to improve case selection, based on 1568 patients. Association Francaise de Chirurgie. *Cancer* **77**, 1254-1262 (1996).
49. Ayez, N.*, et al.* Is the clinical risk score for patients with colorectal liver metastases still useable in the era of effective neoadjuvant chemotherapy? *Annals of surgical oncology* **18**, 2757-2763 (2011).
50. Bos, J.L.*, et al.* Prevalence of ras gene mutations in human colorectal cancers. *Nature* **327**, 293-297 (1987).
51. Karapetis, C.S.*, et al.* K-ras mutations and benefit from cetuximab in advanced colorectal cancer. *The New England journal of medicine* **359**, 1757-1765 (2008).
52. De Roock, W., De Vriendt, V., Normanno, N., Ciardiello, F. & Tejpar, S. KRAS, BRAF, PIK3CA, and PTEN mutations: implications for targeted therapies in metastatic colorectal cancer. *The Lancet. Oncology* **12**, 594-603 (2011).
53. Lee, D.W.*, et al.* KRAS mutation is associated with worse prognosis in stage III or high-risk stage II colon cancer patients treated with adjuvant FOLFOX. *Annals of surgical oncology* **22**, 187-194 (2015).
54. de Cuba, E.M.*, et al.* Prognostic value of BRAF and KRAS mutation status in stage II and III microsatellite instable colon cancers. *International journal of cancer. Journal international du cancer* (2015).
55. Ribic, C.M.*, et al.* Tumor microsatellite-instability status as a predictor of benefit from fluorouracil-based adjuvant chemotherapy for colon cancer. *The New England journal of medicine* **349**, 247-257 (2003).
56. Chan, G.*, et al.* Pathological response grade of colorectal liver metastases treated with neoadjuvant chemotherapy. *HPB : the official journal of the International Hepato Pancreato Biliary Association* **12**, 277-284 (2010).
57. Aloia, T.*, et al.* Liver histology and surgical outcomes after preoperative chemotherapy with fluorouracil plus oxaliplatin in colorectal cancer liver metastases. *Journal of clinical oncology : official journal of the American Society of Clinical Oncology* **24**, 4983-4990 (2006).
58. Chun, Y.S., Laurent, A., Maru, D. & Vauthey, J.N. Management of chemotherapy-associated hepatotoxicity in colorectal liver metastases. *The Lancet. Oncology* **10**, 278-286 (2009).
59. Mentha, G.*, et al.* Dangerous halo after neoadjuvant chemotherapy and two-step hepatectomy for colorectal liver metastases. *The British journal of surgery* **96**, 95-103 (2009).
60. Adam, R.*, et al.* Complete pathologic response after preoperative chemotherapy for colorectal liver metastases: myth or reality? *Journal of clinical oncology : official journal of the American Society of Clinical Oncology* **26**, 1635-1641 (2008).
61. Tanaka, K.*, et al.* Importance of complete pathologic response to prehepatectomy chemotherapy in treating colorectal cancer metastases. *Annals of surgery* **250**, 935-942 (2009).
62. Rubbia-Brandt, L.*, et al.* Importance of histological tumor response assessment in predicting the outcome in patients with colorectal liver metastases treated with neo-adjuvant chemotherapy followed by liver surgery. *Annals of oncology : official journal of the European Society for Medical Oncology / ESMO* **18**, 299-304 (2007).
63. Blazer, D.G., 3rd*, et al.* Pathologic response to preoperative chemotherapy: a new outcome end point after resection of hepatic colorectal metastases. *Journal of*

clinical oncology : official journal of the American Society of Clinical Oncology **26**, 5344-5351 (2008).
64. Dede, K., Salamon, F., Landherr, L., Jakab, F. & Bursics, A. Pathologic assessment of response to chemotherapy in colorectal cancer liver metastases after hepatic resection: which method to use? *Pathology oncology research : POR* **21**, 173-179 (2015).
65. Chang, H.H., Leeper, W.R., Chan, G., Quan, D. & Driman, D.K. Infarct-like necrosis: a distinct form of necrosis seen in colorectal carcinoma liver metastases treated with perioperative chemotherapy. *The American journal of surgical pathology* **36**, 570-576 (2012).
66. Netto, G.J., Eisenberger, M., Epstein, J.I. & Investigators, T.A.X.T. Interobserver variability in histologic evaluation of radical prostatectomy between central and local pathologists: findings of TAX 3501 multinational clinical trial. *Urology* **77**, 1155-1160 (2011).
67. Lozanski, G.*, et al.* Inter-reader variability in follicular lymphoma grading: Conventional and digital reading. *Journal of pathology informatics* **4**, 30 (2013).
68. Thomas, A.*, et al.* Histology-driven data mining of lipid signatures from multiple imaging mass spectrometry analyses: application to human colorectal cancer liver metastasis biopsies. *Analytical chemistry* **85**, 2860-2866 (2013).
69. Vickerman, J.C. Molecular imaging and depth profiling by mass spectrometry--SIMS, MALDI or DESI? *The Analyst* **136**, 2199-2217 (2011).
70. Triolo, A., Altamura, M., Cardinali, F., Sisto, A. & Maggi, C.A. Mass spectrometry and combinatorial chemistry: a short outline. *Journal of mass spectrometry : JMS* **36**, 1249-1259 (2001).
71. Biemann, K. Mass Spectrometry. *Annual review of biochemistry* **32**, 755-780 (1963).
72. VanLear, G.E. & McLafferty, F.W. Biochemical aspects of high-resolution mass spectrometry. *Annual review of biochemistry* **38**, 289-322 (1969).
73. Glish, G.L. & Vachet, R.W. The basics of mass spectrometry in the twenty-first century. *Nature reviews. Drug discovery* **2**, 140-150 (2003).
74. Finehout, E.J. & Lee, K.H. An introduction to mass spectrometry applications in biological research. *Biochemistry and molecular biology education : a bimonthly publication of the International Union of Biochemistry and Molecular Biology* **32**, 93-100 (2004).
75. Aebersold, R. & Mann, M. Mass spectrometry-based proteomics. *Nature* **422**, 198-207 (2003).
76. Harkewicz, R. & Dennis, E.A. Applications of mass spectrometry to lipids and membranes. *Annual review of biochemistry* **80**, 301-325 (2011).
77. Ellis, S.R., Brown, S.H., In Het Panhuis, M., Blanksby, S.J. & Mitchell, T.W. Surface analysis of lipids by mass spectrometry: more than just imaging. *Progress in lipid research* **52**, 329-353 (2013).
78. Norris, J.L. & Caprioli, R.M. Analysis of tissue specimens by matrix-assisted laser desorption/ionization imaging mass spectrometry in biological and clinical research. *Chemical reviews* **113**, 2309-2342 (2013).
79. Chughtai, K. & Heeren, R.M. Mass spectrometric imaging for biomedical tissue analysis. *Chemical reviews* **110**, 3237-3277 (2010).
80. Chaurand, P. Imaging mass spectrometry of thin tissue sections: a decade of collective efforts. *Journal of proteomics* **75**, 4883-4892 (2012).

81. Tanaka, K.*, et al.* Protein and polymer analyses up to m/z 100 000 by laser ionization time-of-flight mass spectrometry. *Rapid Communications in Mass Spectrometry* **2**, 151-153 (1988).
82. Thomas, A., Charbonneau, J.L., Fournaise, E. & Chaurand, P. Sublimation of new matrix candidates for high spatial resolution imaging mass spectrometry of lipids: enhanced information in both positive and negative polarities after 1,5-diaminonapthalene deposition. *Analytical chemistry* **84**, 2048-2054 (2012).
83. Marvin, L.F., Roberts, M.A. & Fay, L.B. Matrix-assisted laser desorption/ionization time-of-flight mass spectrometry in clinical chemistry. *Clinica chimica acta; international journal of clinical chemistry* **337**, 11-21 (2003).
84. Fahy E, S.M., Cotter D and Subramaniam S. . LIPID MAPS online tools for lipid research. . Vol. 35 W606-612 (Nucleic Acids Research, 2007).
85. Desiere. The PeptideAtlas Project. Vol. 34 D655-D658 (Nucleic Acids Research, 2006).
86. McLafferty, F.W. Tandem mass spectrometry. *Science* **214**, 280-287 (1981).
87. Weickhardt, C., Moritz, F. and Grotemeyer, J. Time-of-flight mass spectrometry: State-of the-art in chemical analysis and molecular science. *Mass Spectrom. Rev.* **15**, 139–162 (1996).
88. Lavigne, J.P.*, et al.* Mass spectrometry: a revolution in clinical microbiology? *Clinical chemistry and laboratory medicine* **51**, 257-270 (2013).
89. Spener, F., Lagarde, M., Géloên, A. & Record, M. Editorial: What is lipidomics? *European Journal of Lipid Science and Technology* **105**, 481-482 (2003).
90. Han, X. & Gross, R.W. Global analyses of cellular lipidomes directly from crude extracts of biological samples by ESI mass spectrometry: a bridge to lipidomics. *Journal of lipid research* **44**, 1071-1079 (2003).
91. Cooper, M.J. & Anders, M.W. High Pressure Liquid Chromatography of Fatty Acids and Lipids. *Journal of Chromatographic Science* **13**, 407-411 (1975).
92. Fahy, E.*, et al.* A comprehensive classification system for lipids. *Journal of lipid research* **46**, 839-861 (2005).
93. Goni, F.M. The basic structure and dynamics of cell membranes: an update of the Singer-Nicolson model. *Biochimica et biophysica acta* **1838**, 1467-1476 (2014).
94. Dowhan, W. Molecular basis for membrane phospholipid diversity: why are there so many lipids? *Annual review of biochemistry* **66**, 199-232 (1997).
95. Shevchenko, A. & Simons, K. Lipidomics: coming to grips with lipid diversity. *Nature reviews. Molecular cell biology* **11**, 593-598 (2010).
96. Bell, R.M., Ballas, L.M. & Coleman, R.A. Lipid topogenesis. *Journal of lipid research* **22**, 391-403 (1981).
97. van Meer, G., Voelker, D.R. & Feigenson, G.W. Membrane lipids: where they are and how they behave. *Nature reviews. Molecular cell biology* **9**, 112-124 (2008).
98. Veatch, S.L.*, et al.* Critical fluctuations in plasma membrane vesicles. *ACS chemical biology* **3**, 287-293 (2008).
99. Daum, G. Lipids of mitochondria. *Biochimica et biophysica acta* **822**, 1-42 (1985).
100. Henneberry, A.L., Wright, M.M. & McMaster, C.R. The major sites of cellular phospholipid synthesis and molecular determinants of Fatty Acid and lipid head group specificity. *Molecular biology of the cell* **13**, 3148-3161 (2002).
101. Li, Z.*, et al.* Inhibition of sphingomyelin synthase (SMS) affects intracellular sphingomyelin accumulation and plasma membrane lipid organization. *Biochimica et biophysica acta* **1771**, 1186-1194 (2007).

102. Lingwood, D. & Simons, K. Lipid rafts as a membrane-organizing principle. *Science* **327**, 46-50 (2010).
103. Devaux, P.F. & Morris, R. Transmembrane asymmetry and lateral domains in biological membranes. *Traffic* **5**, 241-246 (2004).
104. Medes, G., Thomas, A. & Weinhouse, S. Metabolism of neoplastic tissue. IV. A study of lipid synthesis in neoplastic tissue slices in vitro. *Cancer research* **13**, 27-29 (1953).
105. Kuhajda, F.P.*, et al.* Fatty acid synthesis: a potential selective target for antineoplastic therapy. *Proceedings of the National Academy of Sciences of the United States of America* **91**, 6379-6383 (1994).
106. Costello, L.C. & Franklin, R.B. 'Why do tumour cells glycolyse?': from glycolysis through citrate to lipogenesis. *Molecular and cellular biochemistry* **280**, 1-8 (2005).
107. Swinnen, J.V.*, et al.* Fatty acid synthase drives the synthesis of phospholipids partitioning into detergent-resistant membrane microdomains. *Biochemical and biophysical research communications* **302**, 898-903 (2003).
108. Lin, R.*, et al.* Acetylation stabilizes ATP-citrate lyase to promote lipid biosynthesis and tumor growth. *Molecular cell* **51**, 506-518 (2013).
109. Abramson, H.N. The lipogenesis pathway as a cancer target. *Journal of medicinal chemistry* **54**, 5615-5638 (2011).
110. Puig, T.*, et al.* Novel Inhibitors of Fatty Acid Synthase with Anticancer Activity. *Clinical cancer research : an official journal of the American Association for Cancer Research* **15**, 7608-7615 (2009).
111. Baenke, F., Peck, B., Miess, H. & Schulze, A. Hooked on fat: the role of lipid synthesis in cancer metabolism and tumour development. *Disease models & mechanisms* **6**, 1353-1363 (2013).
112. Rysman, E.*, et al.* De novo lipogenesis protects cancer cells from free radicals and chemotherapeutics by promoting membrane lipid saturation. *Cancer research* **70**, 8117-8126 (2010).
113. Anhalt, J.P. & Fenselau, C. Identification of bacteria using mass spectrometry. *Analytical chemistry* **47**, 219-225 (1975).
114. Schiller, J.*, et al.* Lipid analysis by matrix-assisted laser desorption and ionization mass spectrometry: A methodological approach. *Analytical biochemistry* **267**, 46-56 (1999).
115. Mapstone, M.*, et al.* Plasma phospholipids identify antecedent memory impairment in older adults. *Nature medicine* **20**, 415-418 (2014).
116. Schiller, J.*, et al.* MALDI-TOF MS in lipidomics. *Frontiers in bioscience : a journal and virtual library* **12**, 2568-2579 (2007).
117. Goto, T.*, et al.* Decreased expression of lysophosphatidylcholine (16:0/OH) in high resolution imaging mass spectrometry independently predicts biochemical recurrence after surgical treatment for prostate cancer. *The Prostate* **75**, 1821-1830 (2015).
118. Jung, J.H.*, et al.* Phospholipids of tumor extracellular vesicles stratify gefitinib-resistant nonsmall cell lung cancer cells from gefitinib-sensitive cells. *Proteomics* **15**, 824-835 (2015).
119. Guo, S.*, et al.* Tissue imaging and serum lipidomic profiling for screening potential biomarkers of thyroid tumors by matrix-assisted laser desorption/ionization-Fourier transform ion cyclotron resonance mass spectrometry. *Analytical and bioanalytical chemistry* **406**, 4357-4370 (2014).

120. Shimma, S.*, et al.* MALDI-based imaging mass spectrometry revealed abnormal distribution of phospholipids in colon cancer liver metastasis. *Journal of chromatography. B, Analytical technologies in the biomedical and life sciences* **855**, 98-103 (2007).
121. Mirnezami, R.*, et al.* Chemical mapping of the colorectal cancer microenvironment via MALDI imaging mass spectrometry (MALDI-MSI) reveals novel cancer-associated field effects. *Molecular oncology* **8**, 39-49 (2014).
122. Lochhead, P.*, et al.* Etiologic field effect: reappraisal of the field effect concept in cancer predisposition and progression. *Modern pathology : an official journal of the United States and Canadian Academy of Pathology, Inc* **28**, 14-29 (2015).
123. Turtoi, A.*, et al.* Organized proteomic heterogeneity in colorectal cancer liver metastases and implications for therapies. *Hepatology* **59**, 924-934 (2014).
124. Rompp, A.*, et al.* imzML: Imaging Mass Spectrometry Markup Language: A common data format for mass spectrometry imaging. *Methods in molecular biology* **696**, 205-224 (2011).
125. Gibb, S. & Strimmer, K. MALDIquant: a versatile R package for the analysis of mass spectrometry data. *Bioinformatics* **28**, 2270-2271 (2012).
126. Alfassi, Z.B. On the normalization of a mass spectrum for comparison of two spectra. *Journal of the American Society for Mass Spectrometry* **15**, 385-387 (2004).
127. Yang, C., He, Z. & Yu, W. Comparison of public peak detection algorithms for MALDI mass spectrometry data analysis. *BMC Bioinformatics* **10**, 1-13 (2009).
128. Bemis, K.D.*, et al.* Cardinal: an R package for statistical analysis of mass spectrometry-based imaging experiments. *Bioinformatics* **31**, 2418-2420 (2015).
129. Alexandrov, T. & Kobarg, J.H. Efficient spatial segmentation of large imaging mass spectrometry datasets with spatially aware clustering. *Bioinformatics* **27**, i230-238 (2011).
130. Le Cao, K.A., Gonzalez, I. & Dejean, S. integrOmics: an R package to unravel relationships between two omics datasets. *Bioinformatics* **25**, 2855-2856 (2009).
131. Sing, T., Sander, O., Beerenwinkel, N. & Lengauer, T. ROCR: visualizing classifier performance in R. *Bioinformatics* **21**, 3940-3941 (2005).
132. Fischer, A.H., Jacobson, K.A., Rose, J. & Zeller, R. Hematoxylin and eosin staining of tissue and cell sections. *CSH protocols* **2008**, pdb prot4986 (2008).
133. Morrissey, S.M. & Tymvios, M.C. Acid mucins in human intestinal goblet cells. *The Journal of pathology* **126**, 197-208 (1978).
134. Jiang, X.C.*, et al.* Expression of plasma phospholipid transfer protein mRNA in normal and emphysematous lungs and regulation by hypoxia. *The Journal of biological chemistry* **273**, 15714-15718 (1998).
135. Ragusa, M.A.*, et al.* RT-PCR and in situ hybridization analysis of apolipoprotein H expression in rat normal tissues. *International journal of molecular medicine* **18**, 449-455 (2006).
136. Kyzer, S. & Gordon, P.H. Determination of proliferative activity in colorectal carcinoma using monoclonal antibody Ki67. *Diseases of the colon and rectum* **40**, 322-325 (1997).
137. Eisenhauer, E.A.*, et al.* New response evaluation criteria in solid tumours: revised RECIST guideline (version 1.1). *European journal of cancer* **45**, 228-247 (2009).
138. Thomas, A., Patterson, N., Dufresne, M. & Chaurand, P. (MA)LDI MS Imaging at High Specificity and Sensitivity. in *Advances in MALDI and Laser-Induced Soft*

Ionization Mass Spectrometry (ed. Cramer, R.) 129-147 (Springer International Publishing, 2016).
139. Cerruti, C.D.*, et al.* MALDI imaging mass spectrometry of lipids by adding lithium salts to the matrix solution. *Analytical and bioanalytical chemistry* **401**, 75-87 (2011).
140. Arana, L., Gangoiti, P., Ouro, A., Trueba, M. & Gomez-Munoz, A. Ceramide and ceramide 1-phosphate in health and disease. *Lipids in health and disease* **9**, 15 (2010).
141. Ogretmen, B. & Hannun, Y.A. Biologically active sphingolipids in cancer pathogenesis and treatment. *Nature reviews. Cancer* **4**, 604-616 (2004).
142. Gomez-Munoz, A., Kong, J.Y., Salh, B. & Steinbrecher, U.P. Ceramide-1-phosphate blocks apoptosis through inhibition of acid sphingomyelinase in macrophages. *Journal of lipid research* **45**, 99-105 (2004).
143. Magnusson, C.D. & Haraldsson, G.G. Ether lipids. *Chemistry and physics of lipids* **164**, 315-340 (2011).
144. Baker, M. Reproducibility crisis: Blame it on the antibodies. *Nature* **521**, 274-276 (2015).
145. Zhao, Z.*, et al.* Plasma lysophosphatidylcholine levels: potential biomarkers for colorectal cancer. *Journal of clinical oncology : official journal of the American Society of Clinical Oncology* **25**, 2696-2701 (2007).

6. APPENDIX

Varible	Training Set			Validation Set		
	No.(%)	Mean (SD)	Range	No.(%)	Mean (SD)	Range
Age (years)		62.7 (15.9)	31-81		*63.2 (11.7)	*40-81
Sex						
Male	5 (41.7)			*26 (68.4)		
Female	7 (58.3)			*12 (31.5)		
Primary Disease						
Proper Colon	4 (33.3)			*11(28.9)		
Sigmoid Colon	4 (33.3)			*5 (13.15)		
Rectum	4 (33.3)			*14 (36.8)		
Unknown	0 (0)			*8 (21)		
Primary Disease (TNM)						
T (size)						
T1	0 (0)			*1 (2.6)		
T2	0 (0)			*2 (5.2)		
T3	7 (58.3)			*20 (52.6)		
T4	4 (33.3)			*4 (10.4)		
Unknown	1 (8.3)			*11 (28.9)		
N (lymph node)						
N0	3 (25)			*8 (21)		
N1	6 (50)			*10 (26.3)		
N2	2 (16.6)			*7 (18.4)		
Unknown	1 (8.3)			*13 (34.2)		
Disease Free intevral						
Synchronous	12 (100)			**21 (52.5)		
Metachrnous	0 (0)			**19 (47.5)		
Location of Liver Lesion						
Right Lobe	9 (75)			**20 (50)		
Lift Lobe	3 (25)			**18 (45)		
Bilobar	0 (0)			**2 (5)		
No. of Lesions		2.1 (1.9)	1-7		**2.6 (1.9)	**1-10
≤ 4	10 (83.3)			**29 (72.5)		
> 4	2 (16.6)			**11 (27.5)		
Size of Lesion (cm)		4.7 (2.3)	0.3-9.2		**3.4 (2.3)	**0.8-10
≤ 5 cm	6 (50)					

		••31(77.5)
> 5 cm	6 (50)	••9 (22.5)
Chemotherapy Status		
Chemo-naive	3 (25)	••14 (35)
Treated	9 (75)	••26 (65)

Table 6.1 : **Patient characteristics separated by training and validation set.** Training set 12 lesions from 12 patients. Validation set 40 lesions from 38 patients (2 patients underwent stage resection). *n=38 **n=40

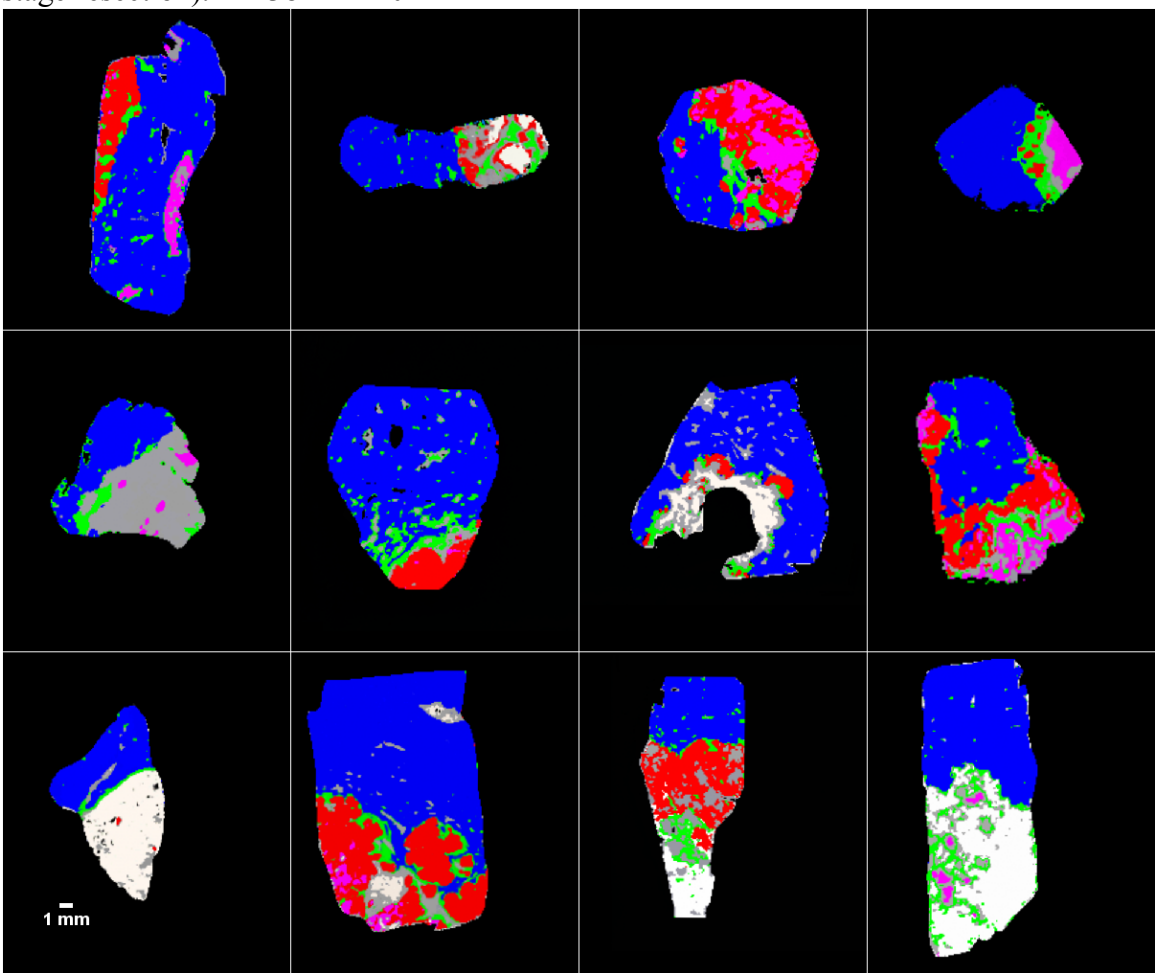

Figure 6.1: Segmentation of the IMS data for the training set. The colors blue, red, purple, green, grey and white represent normal liver, viable tumor, necrosis, inflammation, fibrosis, and mucinous/empty/noise areas in and outside the tumor area, respectively

Figure 6.2 :MS/MS (fragmentation) of most discrimiant markers. Fatty acid side chain length and number of unsaturations are given, however, side chain position at either *sn-1* or *sn-2* is not known.

I. Adjacent "Normal" Liver, Negative mode, *m/z* 738.62, PE(16:0/20:4)

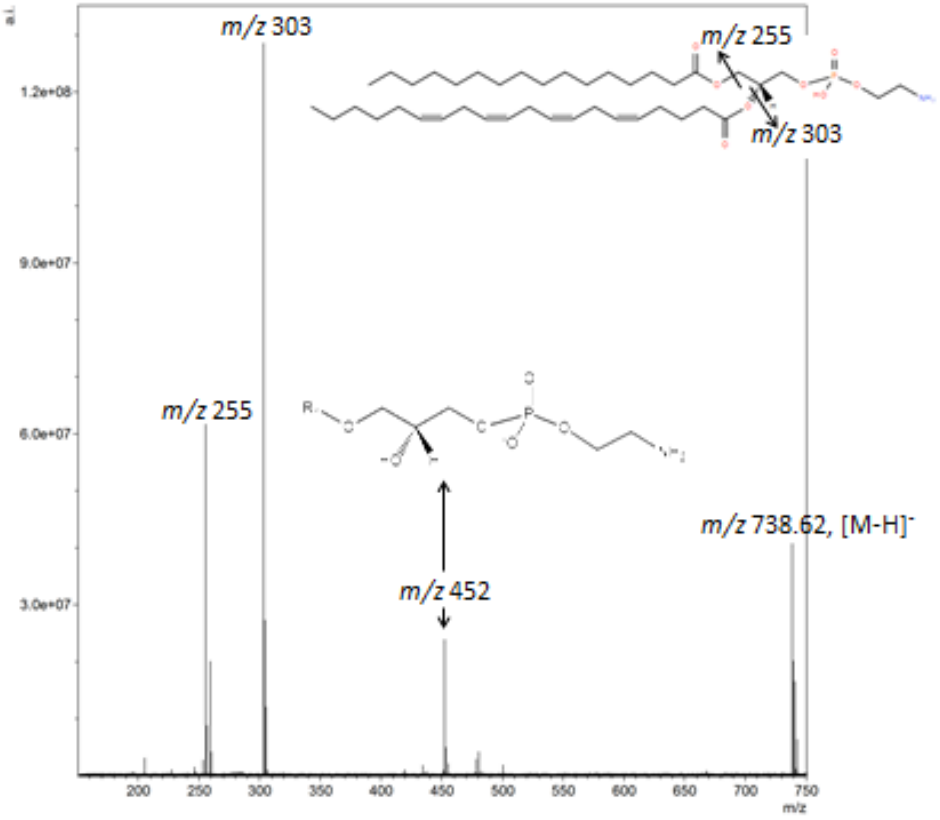

II. Adjacent "Normal" Liver, Negative mode, *m/z* 762.55, PE(16:0/20:4)

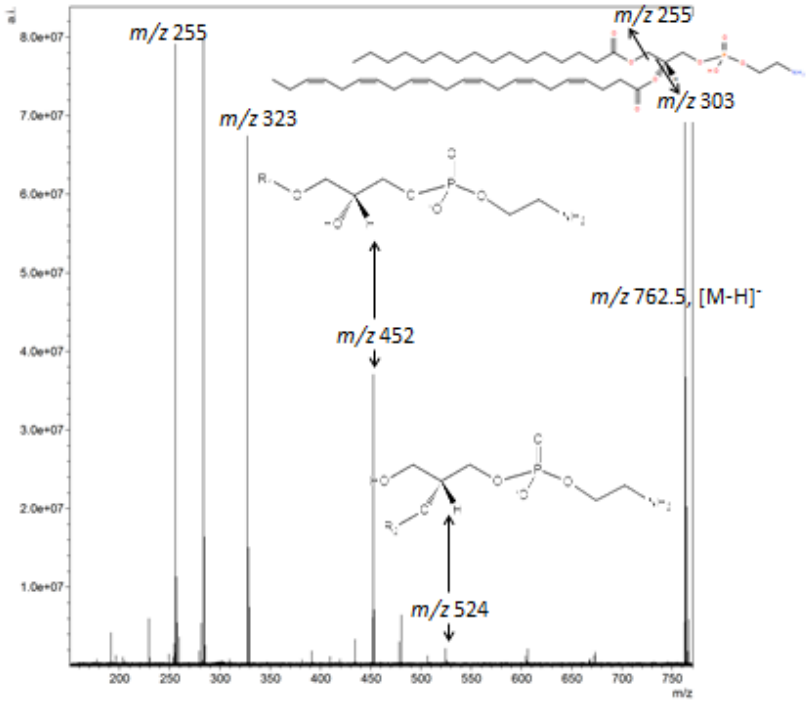

III. Adjacent "Normal" Liver, Negative mode, *m/z* 885.56, PI(18:0/20:4)

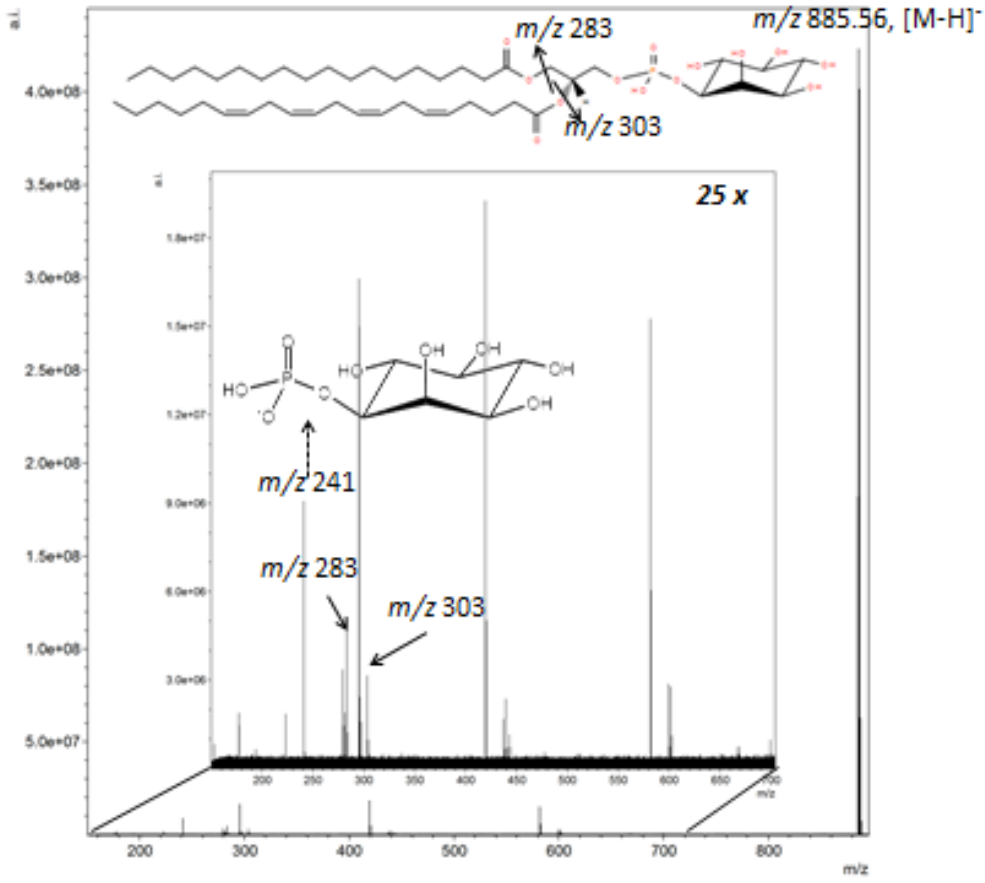

IV. Adjacent "Normal" Liver, Positive mode, *m/z* 758.57, PC(16:0/18:2)

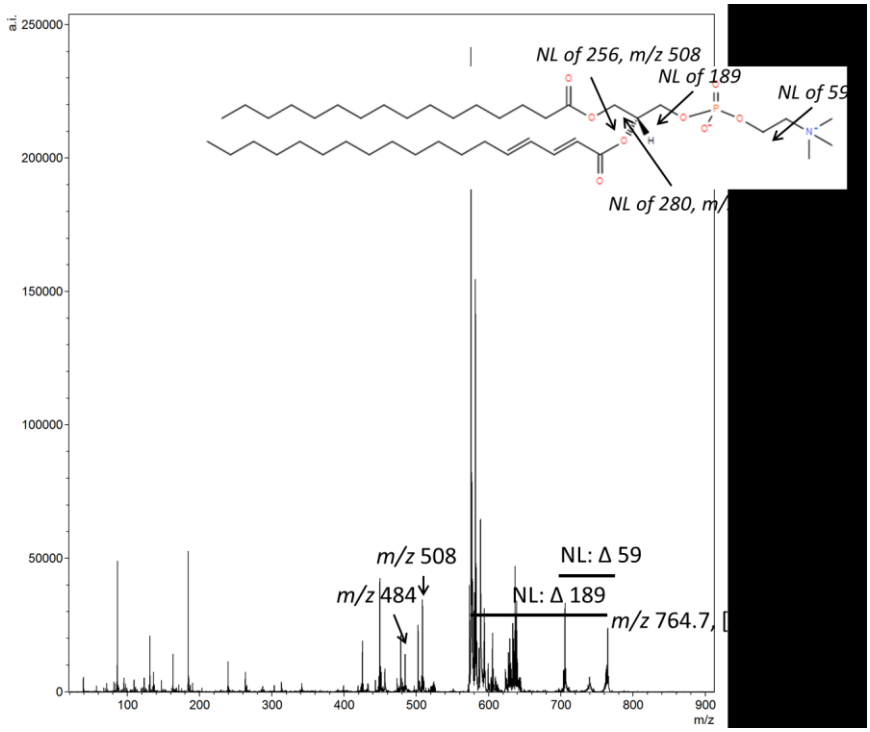

V. Viable Tumor, Negative mode, *m/z* 698.48, PE(p-16:0/18:2)

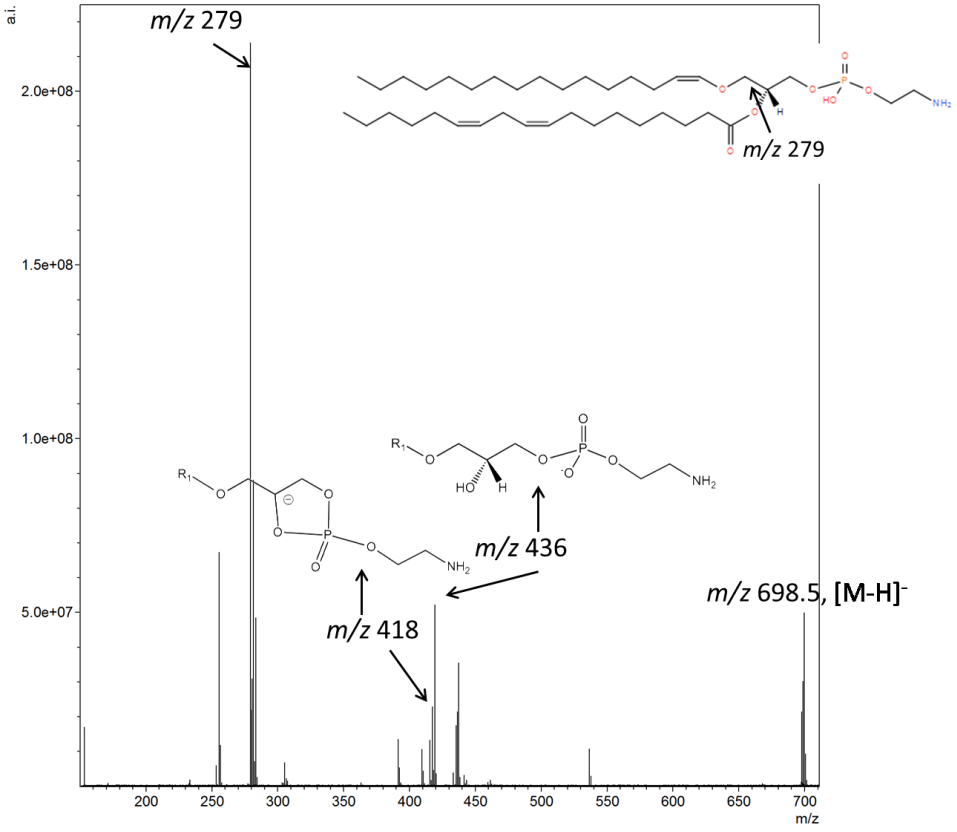

VI. Viable Tumor, Negative mode, *m/z* 700.51, PE(p-16:0/18:1)

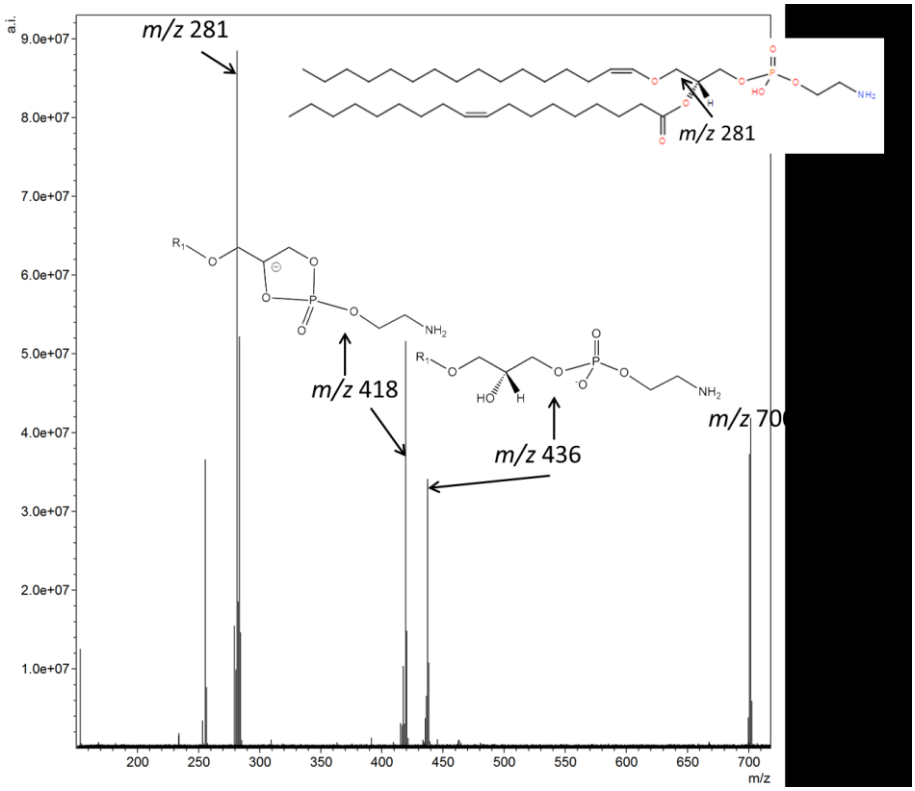

VII. Viable Tumor, Negative mode, *m/z* 835.51, PE(p-16:0/18:1)

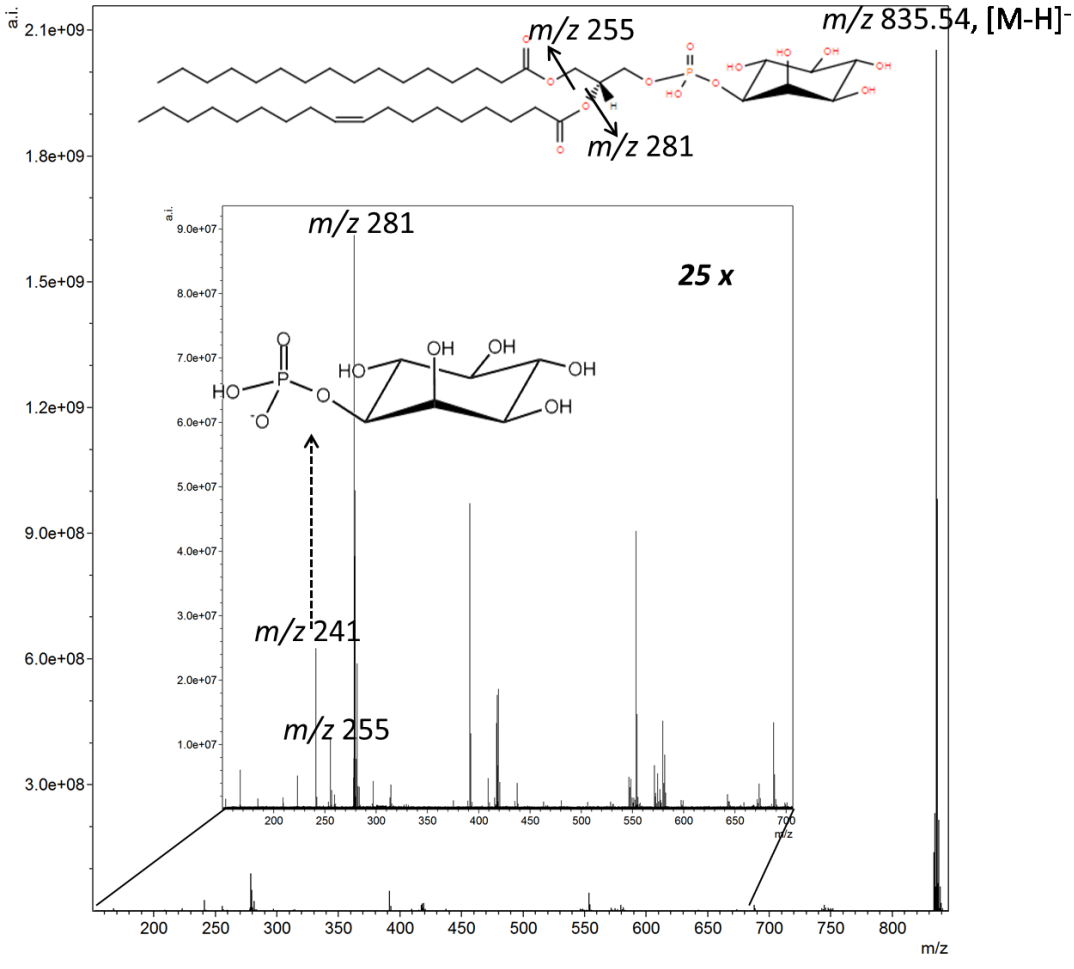

VIII. Viable Tumor, Positive mode, *m/z* 706.55, PC(14:0/16:0) : Identified through LIPIDMAPS on exact mass

IX. Viable Tumor, Positive mode, *m/z* 732.54, PC(16:0/16:1)

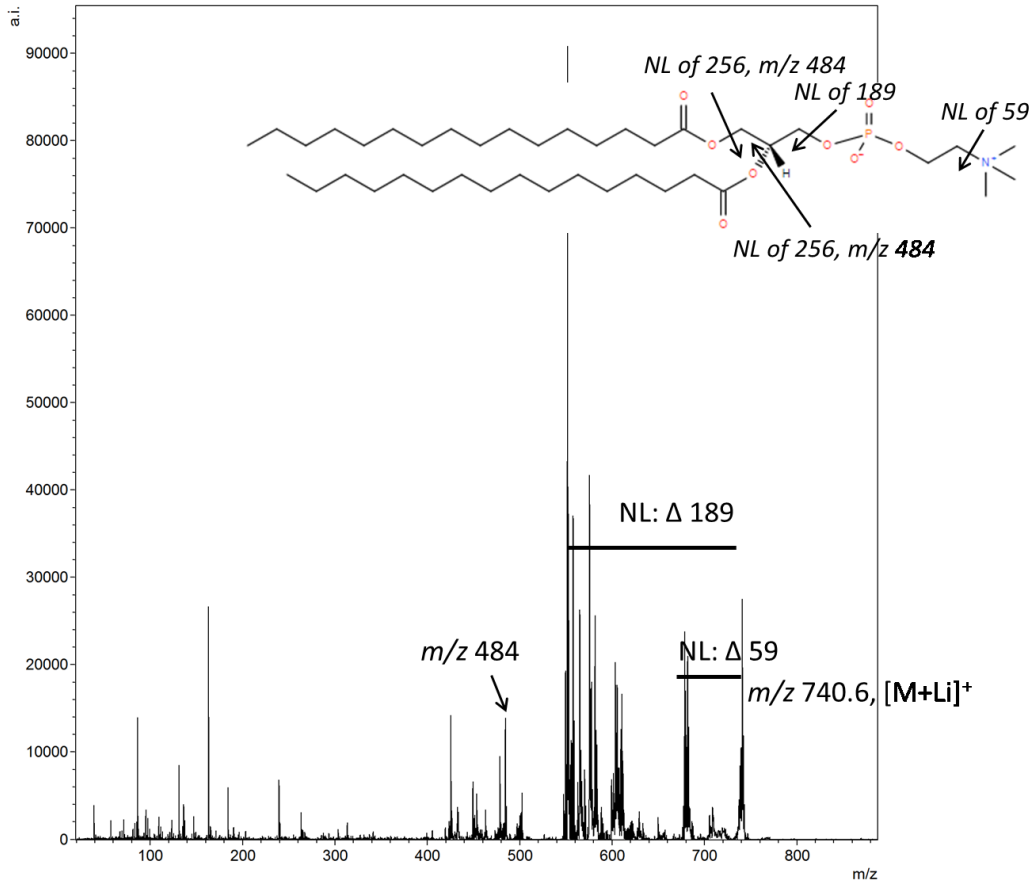

X. Inflammation, Negative Mode, *m/z* 722.49, PE(p-16:0/ 20:4)

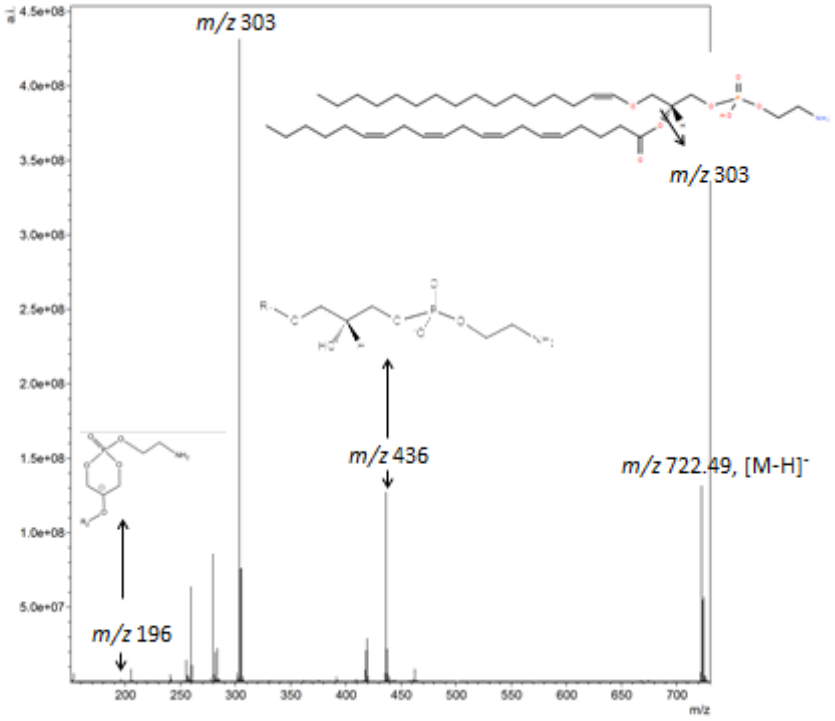

XI. Inflammation, Negative Mode, *m/z* 750.53, PE(p-18:0/ 20:4)

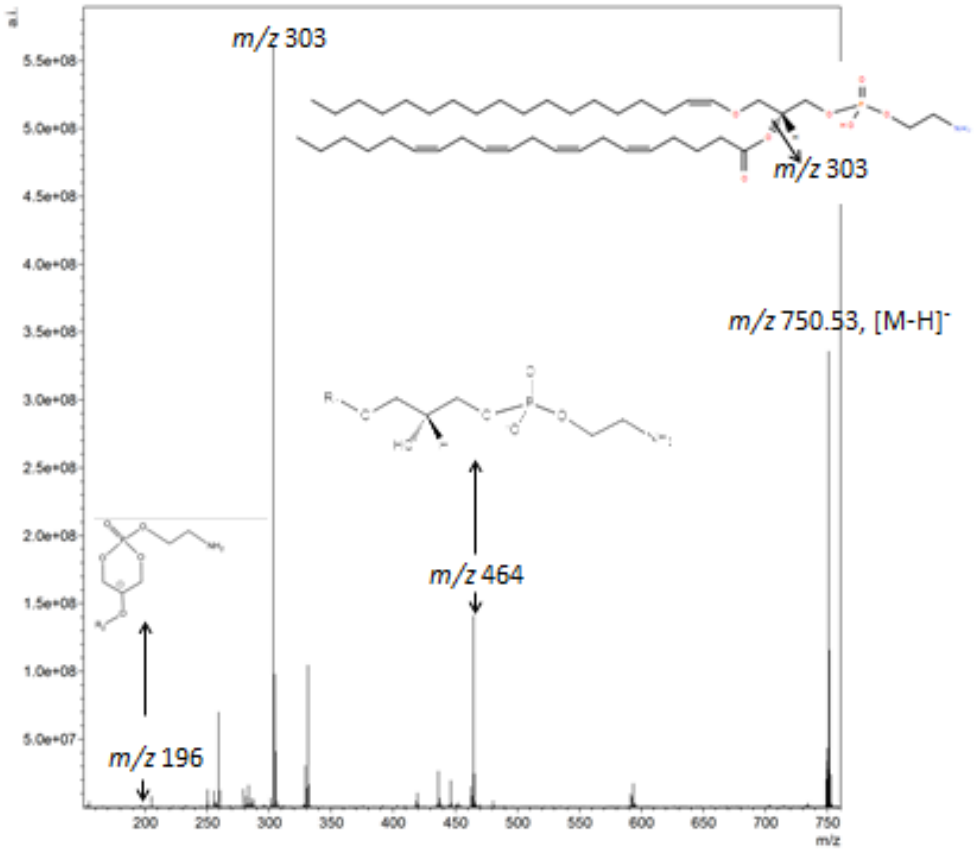

XII. Inflammation, Positive Mode, *m/z* 734.57, PC(16:0/ 16:0)

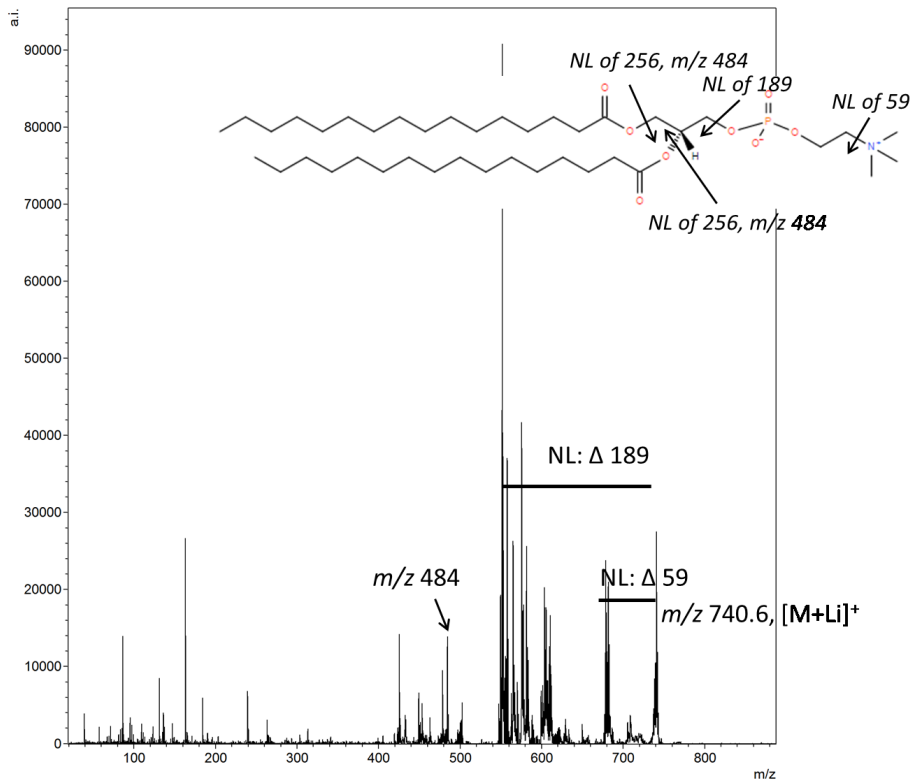

XIII. Necrosis, Positive Mode, *m/z* 703.57, SM(d18:1/16:0)

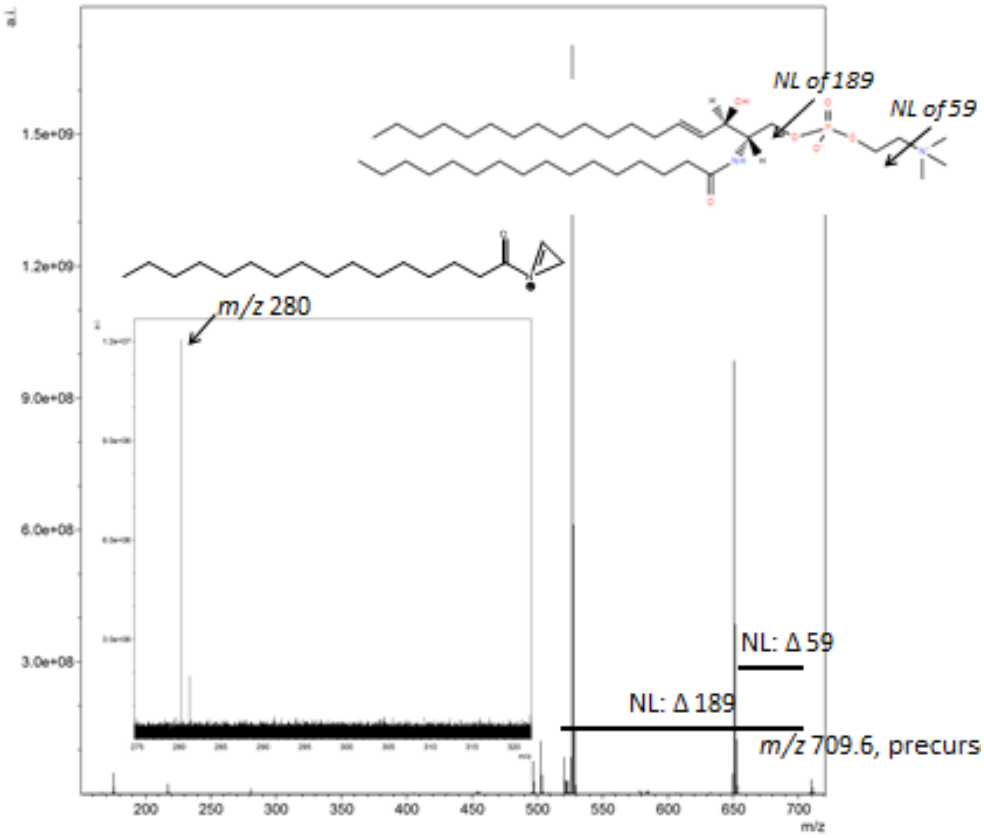

Table 6.2: Pathologists and IMS mTRG gradings for all samples

serial no.	Path1	Path2	IMS
1	1	2	1
2	2	2	2
3	3	3	3
4	3	5	3
5	3	3	3
6	4	4	4
7	4	5	3
8	2	2	1
9	4	4	4
10	4	5	4
11	5	4	4
12	3	4	3
13	3	3	3
14	3	too small to assess	3
15	4	5	3
16	3	too small to assess	3
17	4	5	3
18	4	4	4
19	1	too small to assess	1
20	4	3	3
21	4	4	3
22	2	1	1
23	4	4	4
24	2	1	2
25	3	5	4
26	3	3	4
27	2	too small to assess	3
28	2	2	2
29	3	2	2
30	4	4	3
31	3	3	3
32	4	too small to assess	4
33	3	3	3
34	1	1	1
35	3	2	3
36	3	3	3
37	4	4	4
38	4	4	4
39	4	1	5
40	3	3	3
41	4	4	3
42	4	4	4
43	4	4	3
44	4	4	4
45	4	4	3
46	4	4	4
47	2	2	2
48	3	4	4
49	4	5	4
50	2	2	2
51	3	3	2
52	4	4	4

Figure 6.3: Predictive IMS on validation set of CRC samples. (*a*) For all samples, a is the predicted IMS data at 100 µm. (*b*) large scale view of H&E staining of serial section. (*c-e*) zoom views of H&E for comparison.

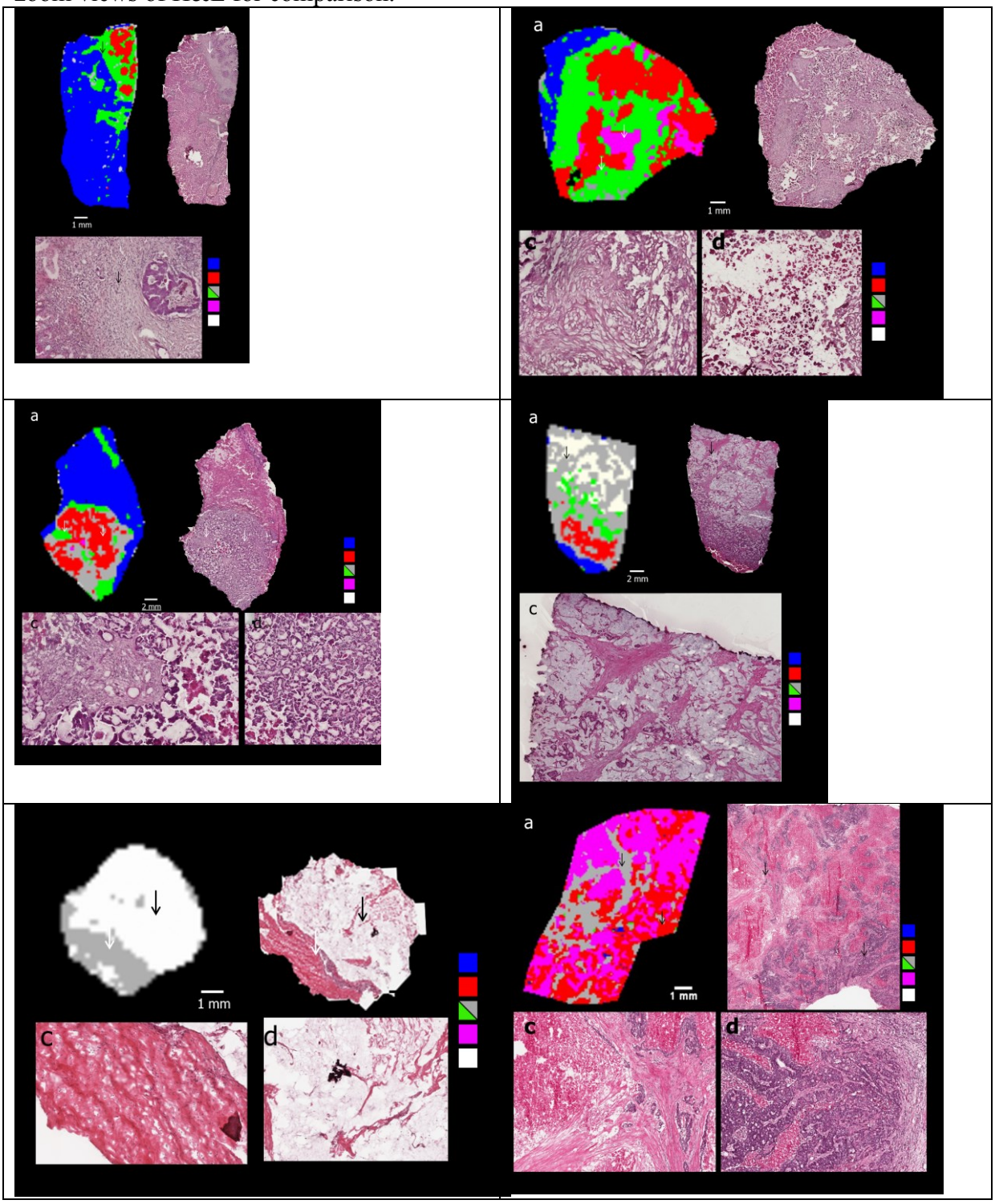

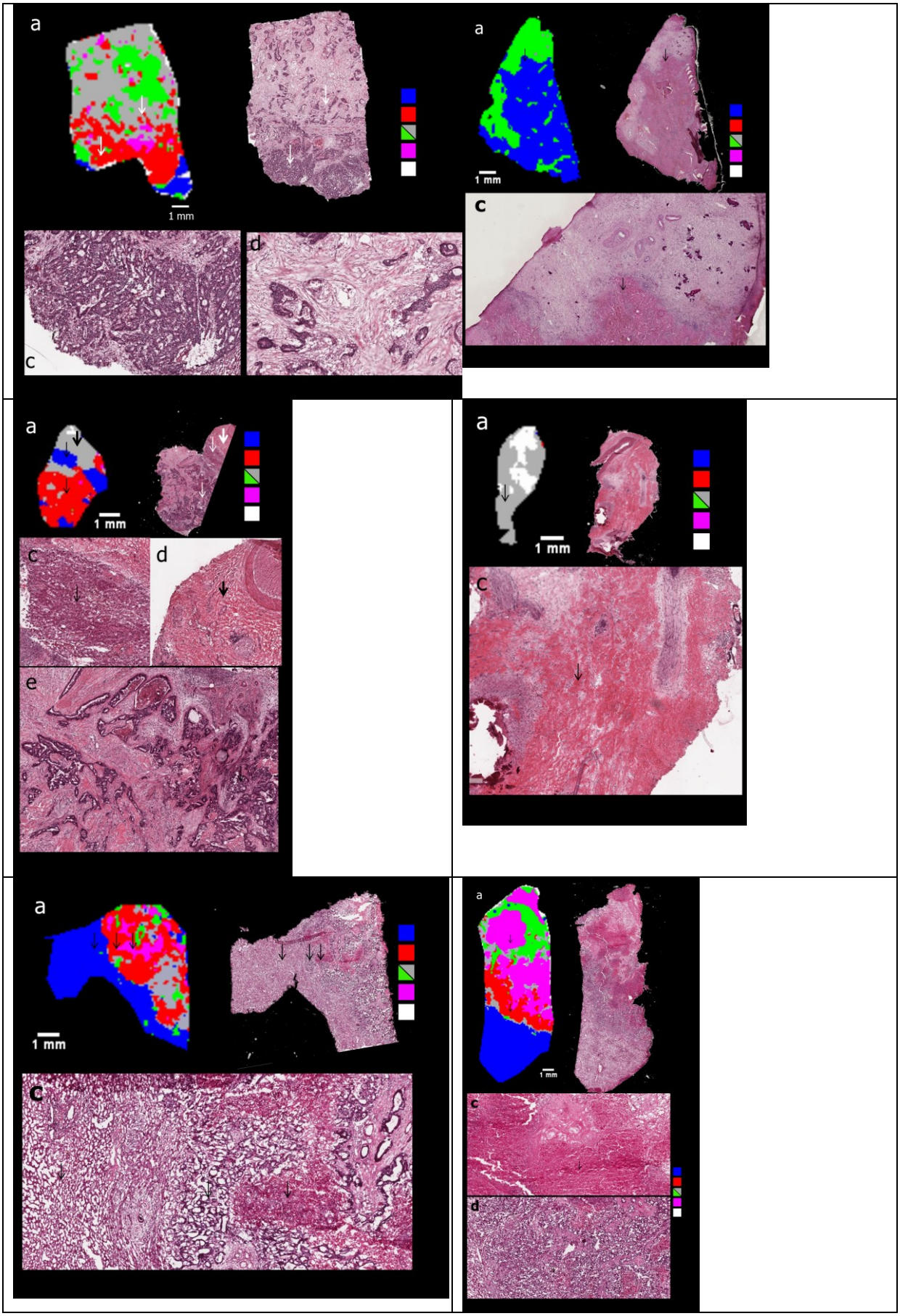
a
1 mm
c
d
a
1 mm
c
a
1 mm
c
d
e
a
1 mm
c
a
1 mm
c
d

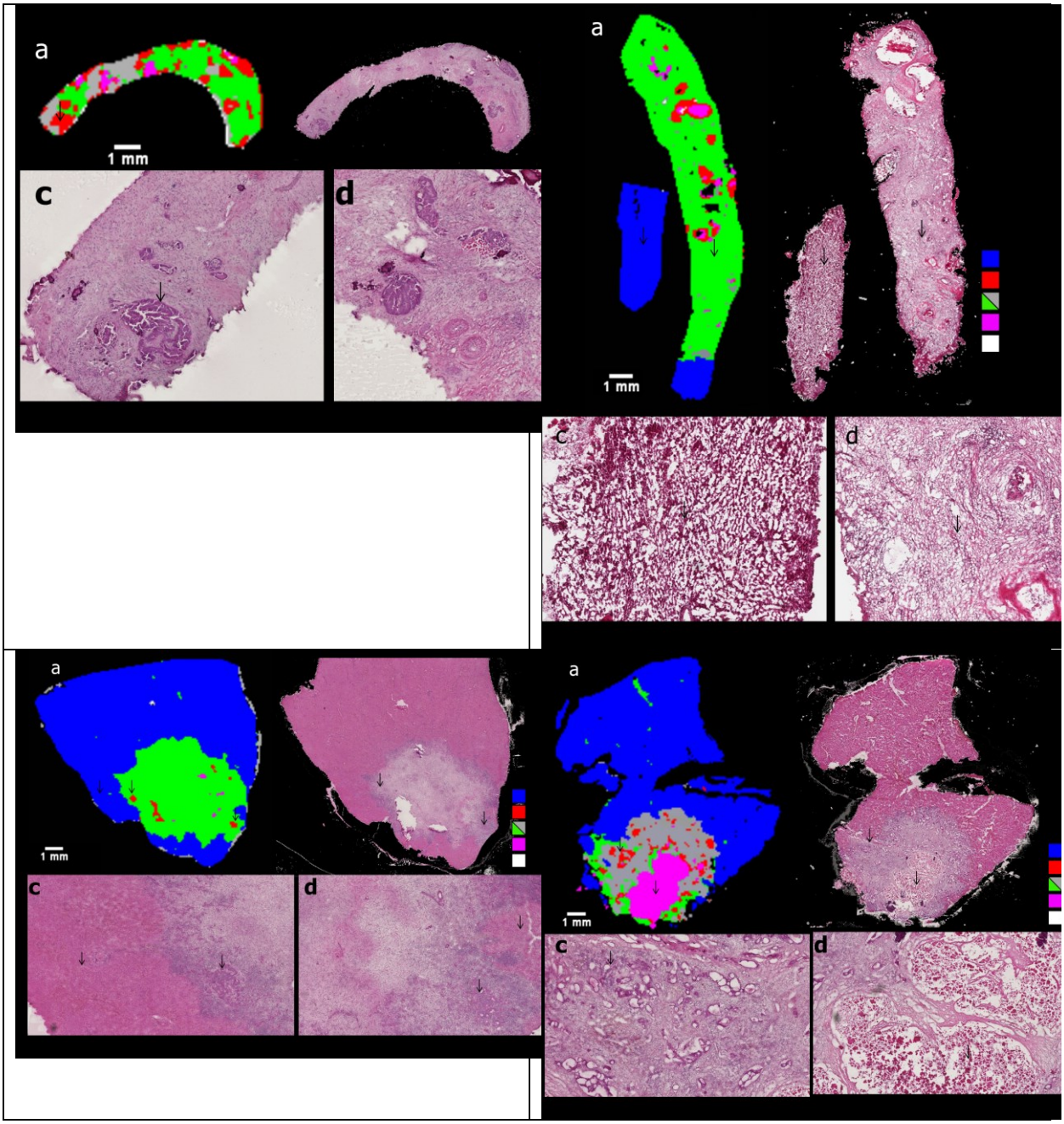
a
1 mm
c
d
a
1 mm
c
d
a
1 mm
c
d
a
1 mm
c
d

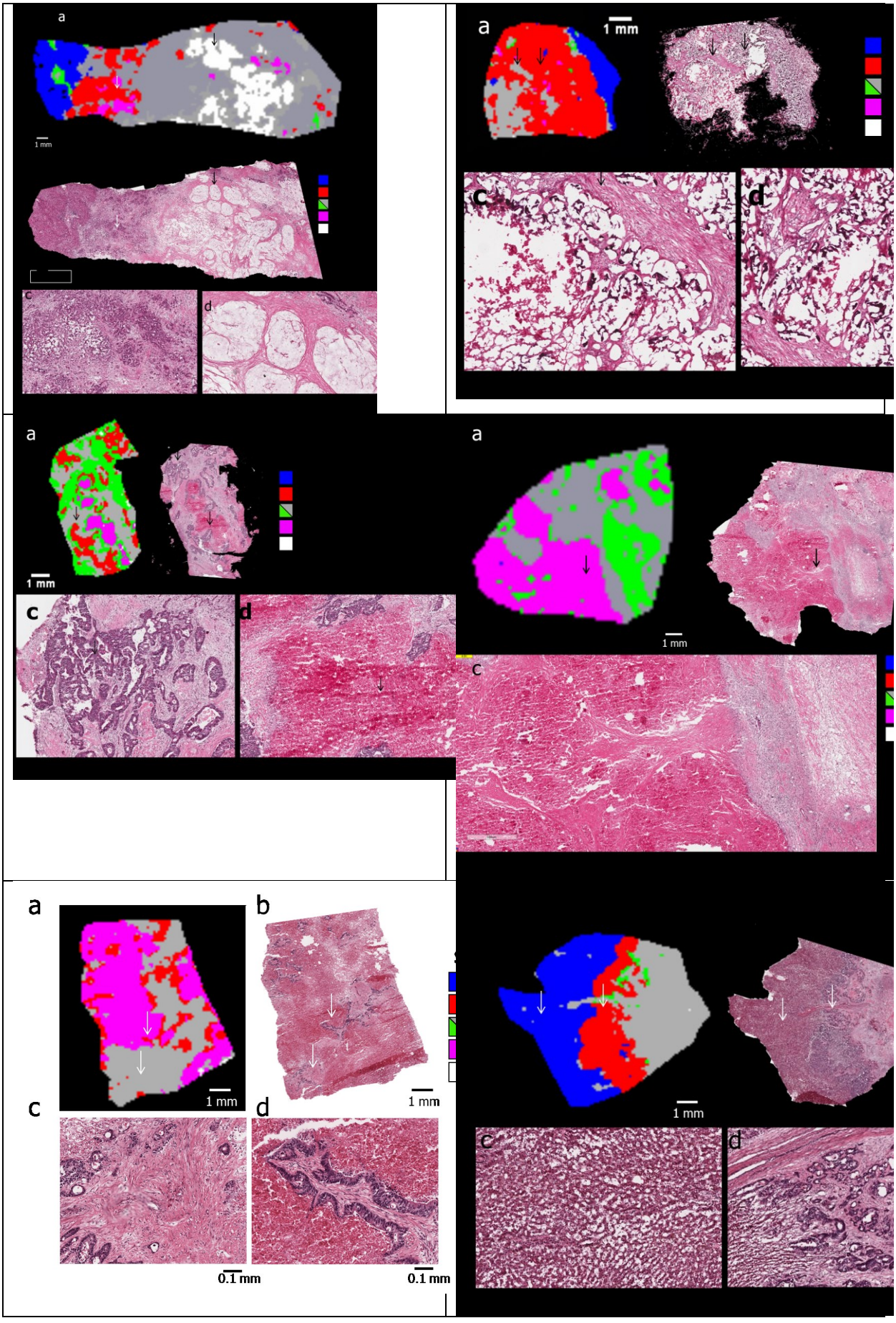
a
1 mm
c
d
a
1 mm
c
d
a
1 mm
c
d
a
1 mm
c
a
b
1 mm
1 mm
c
d
0.1 mm
0.1 mm
a
1 mm
c
d

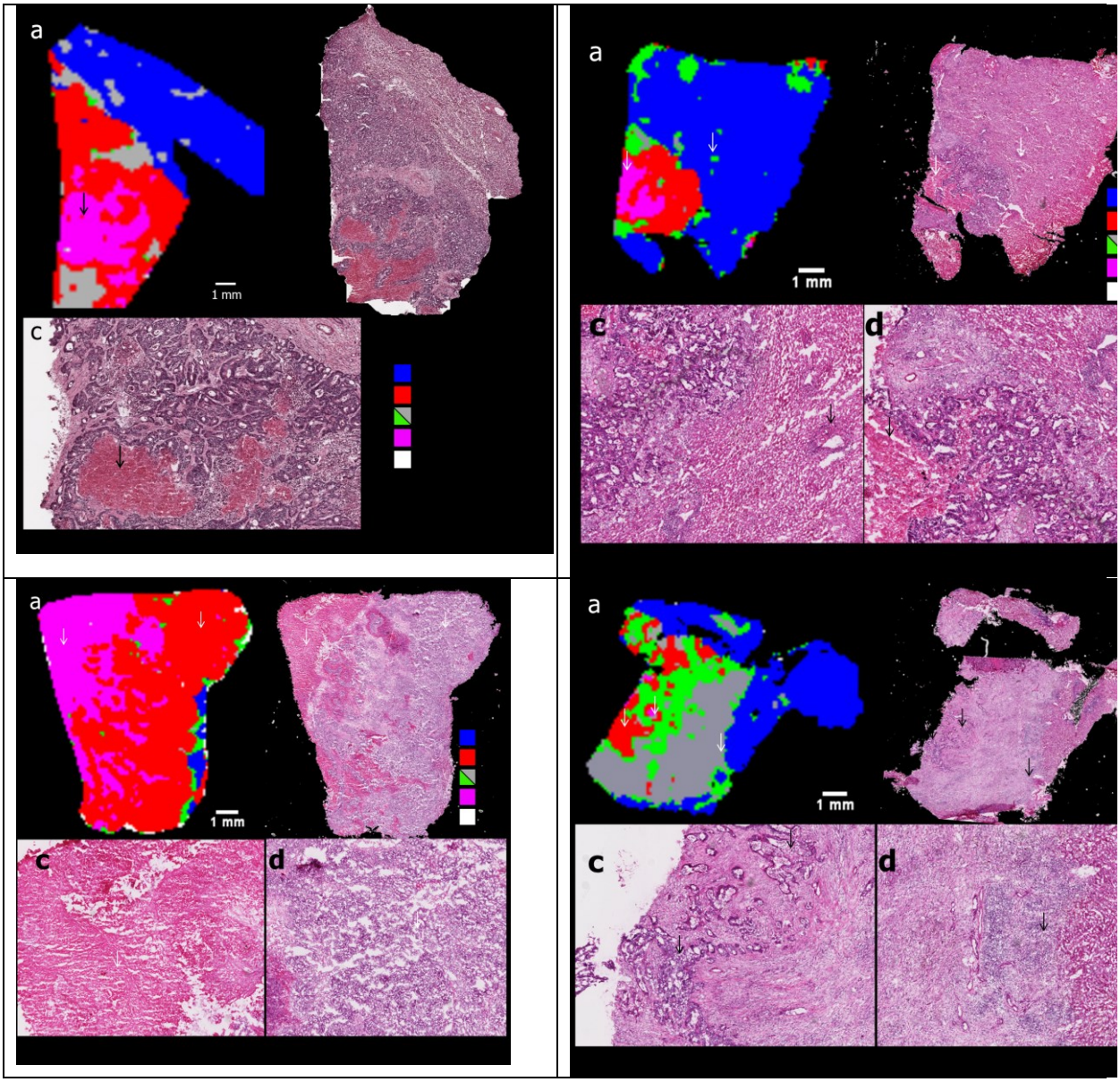
a
1 mm
c
a
1 mm
c
d
a
1 mm
c
d
a
1 mm
c
d

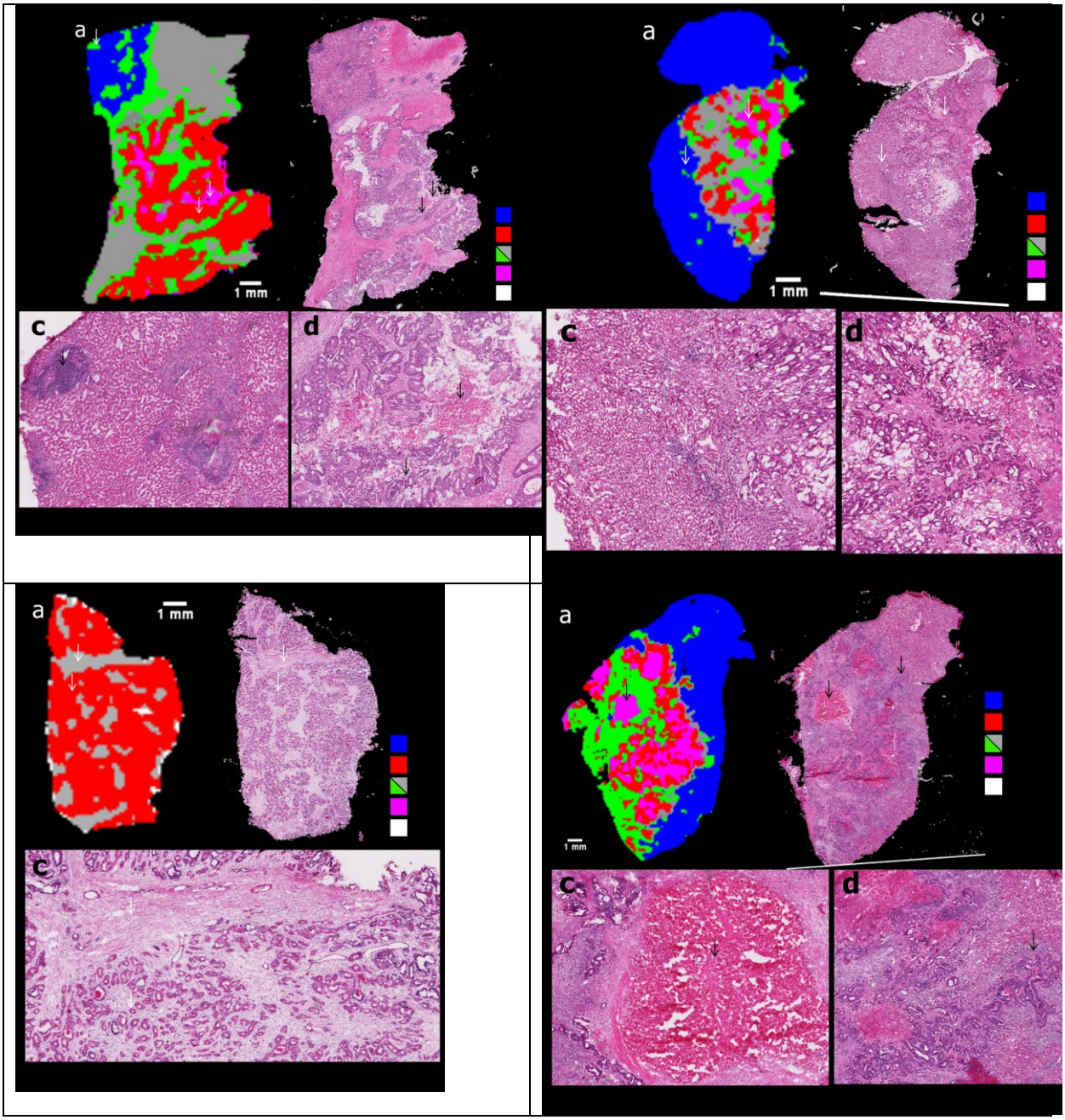
a
1 mm
c
d
a
1 mm
c
d
a
1 mm
c
a
1 mm
c
d

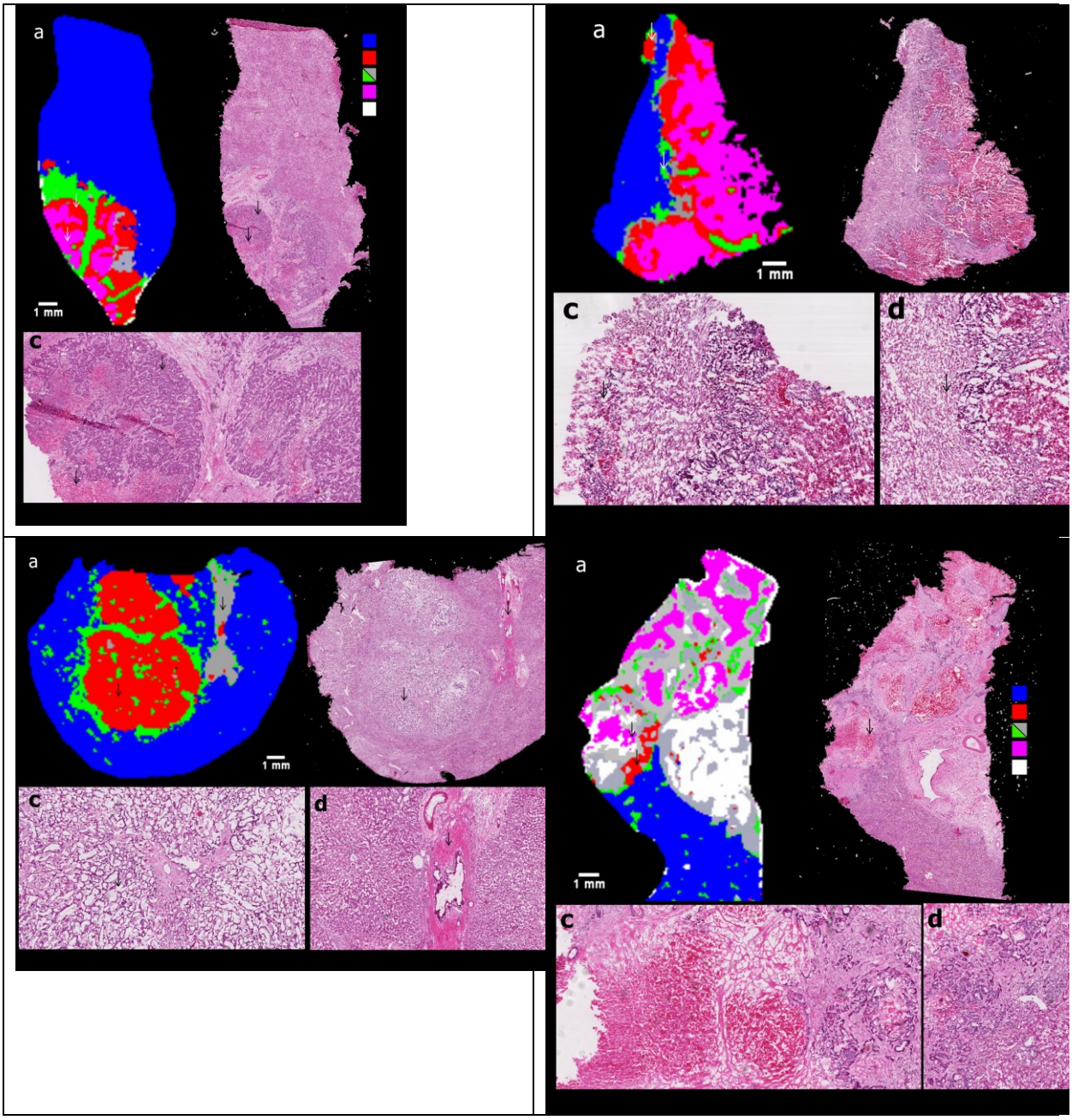
a
1 mm
c
a
1 mm
c
d
a
1 mm
c
d
a
1 mm
c
d

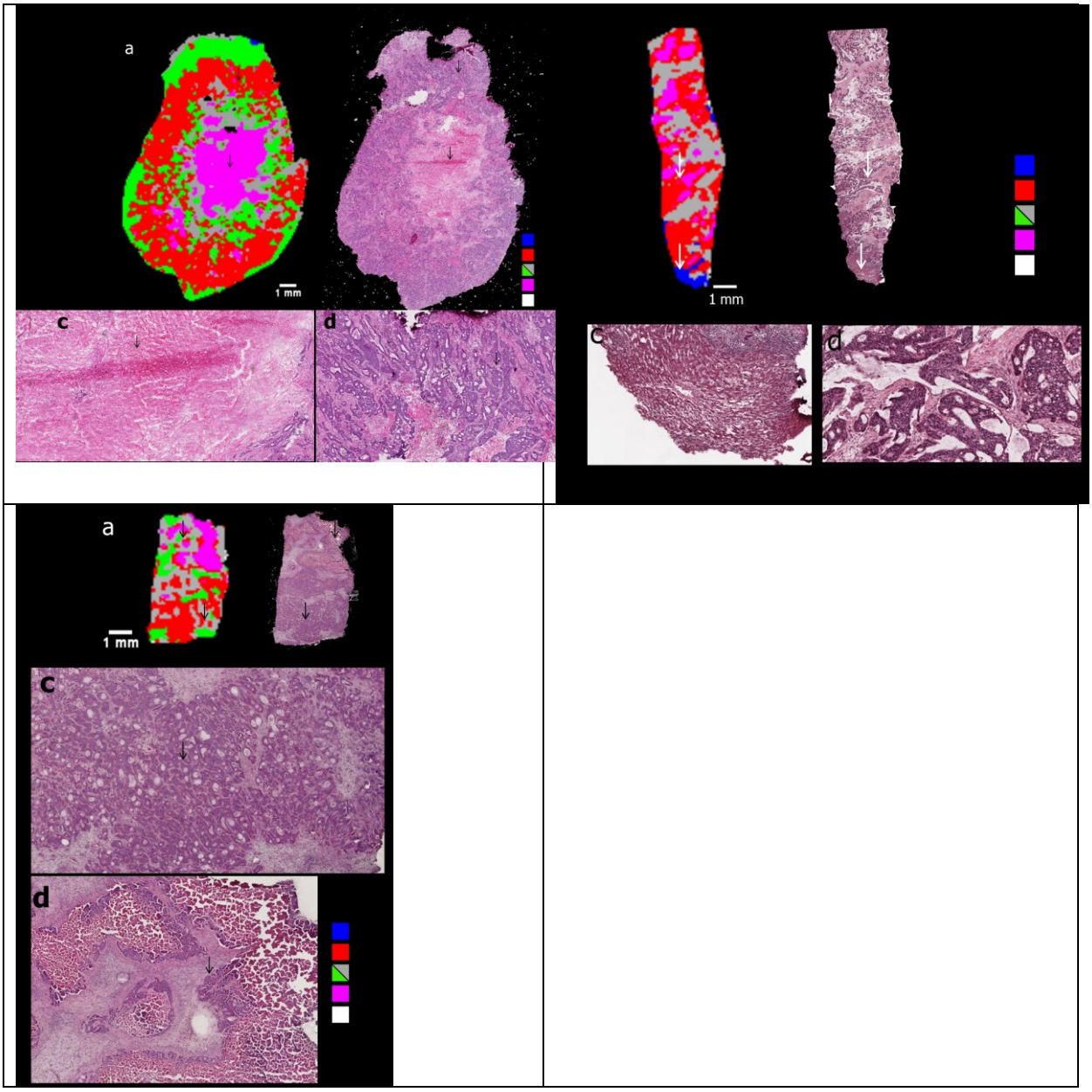

Figure 6.4:Ion images of topographical markers

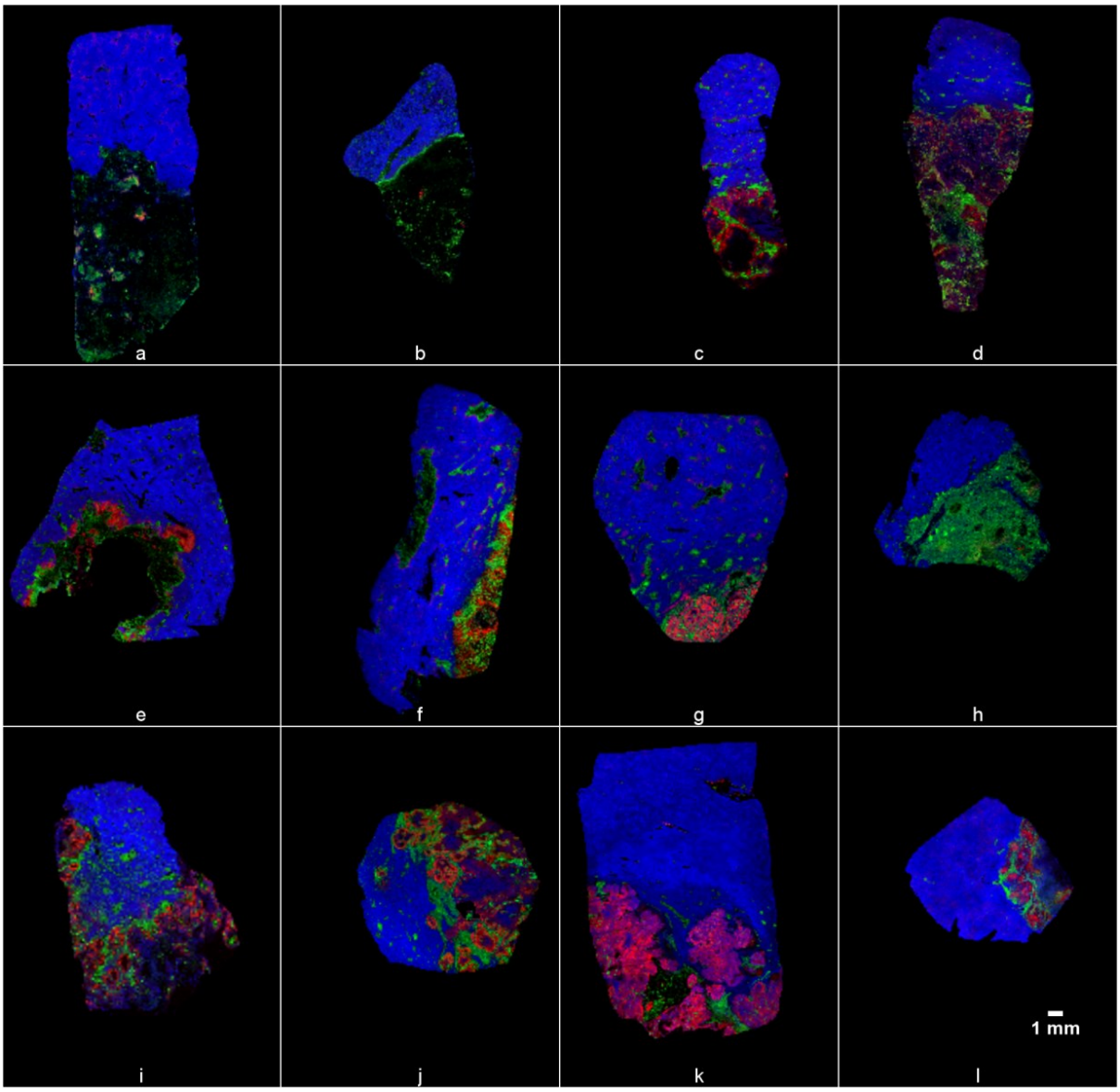

I. Markers of inflammatory cells(green), tumor cells(red), and adjacent liver(blue) from positive ionization mode. Green = + *m/z* 734.56, PC(32:0). Red = + *m/z* 732.55 PC(32:1). Blue = + *m/z* 758.56, PC (34:2).

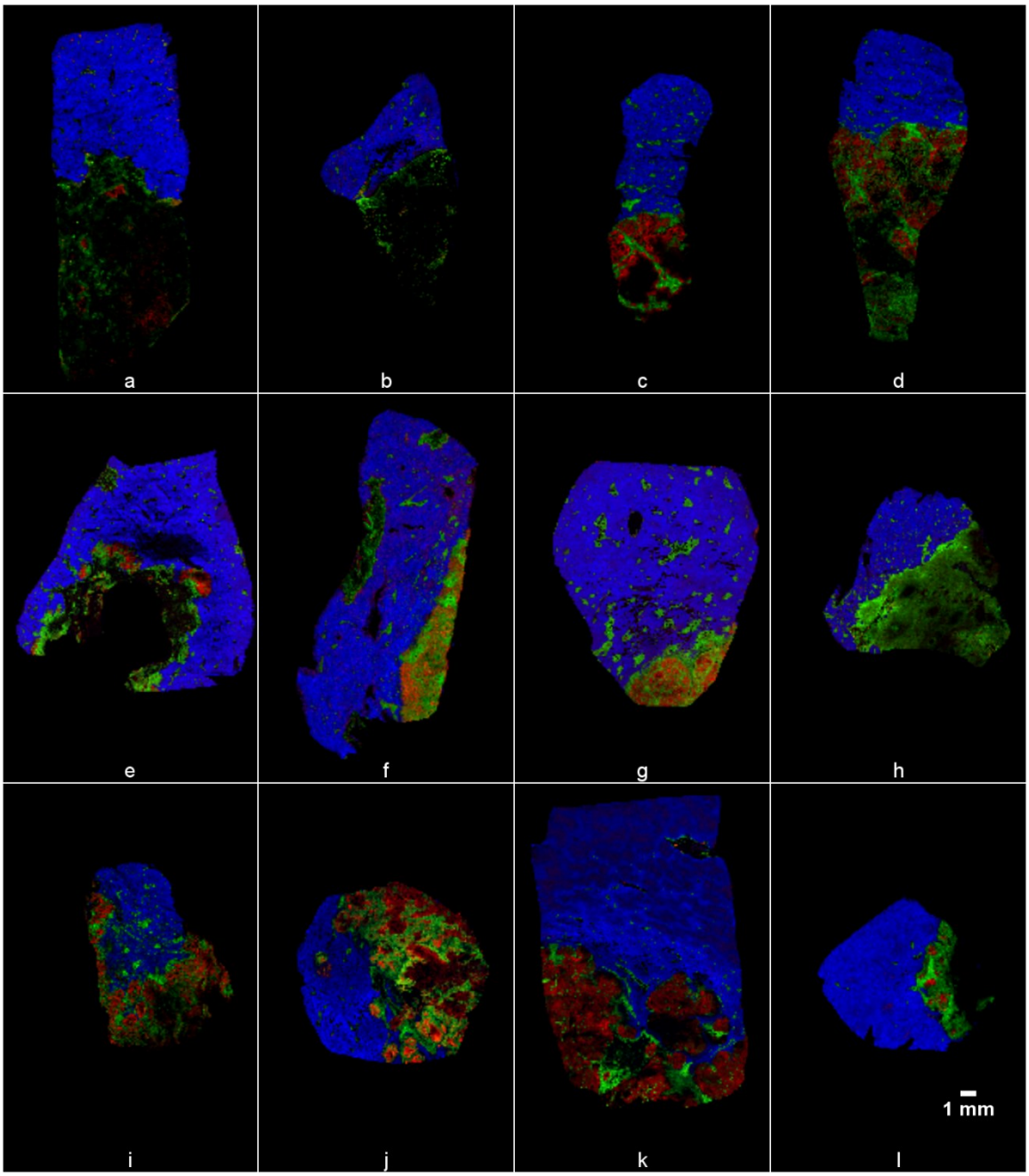

II. Markers of inflammatory cells (green), tumor cells (red), and adjacent liver (blue) from positive ionization mode. Green = - *m/z* 722.51, PE(P-36:4). Red = - *m/z* 700.50 PE(P-34:2). Blue = - *m/z* 762.50, PE(38:6).

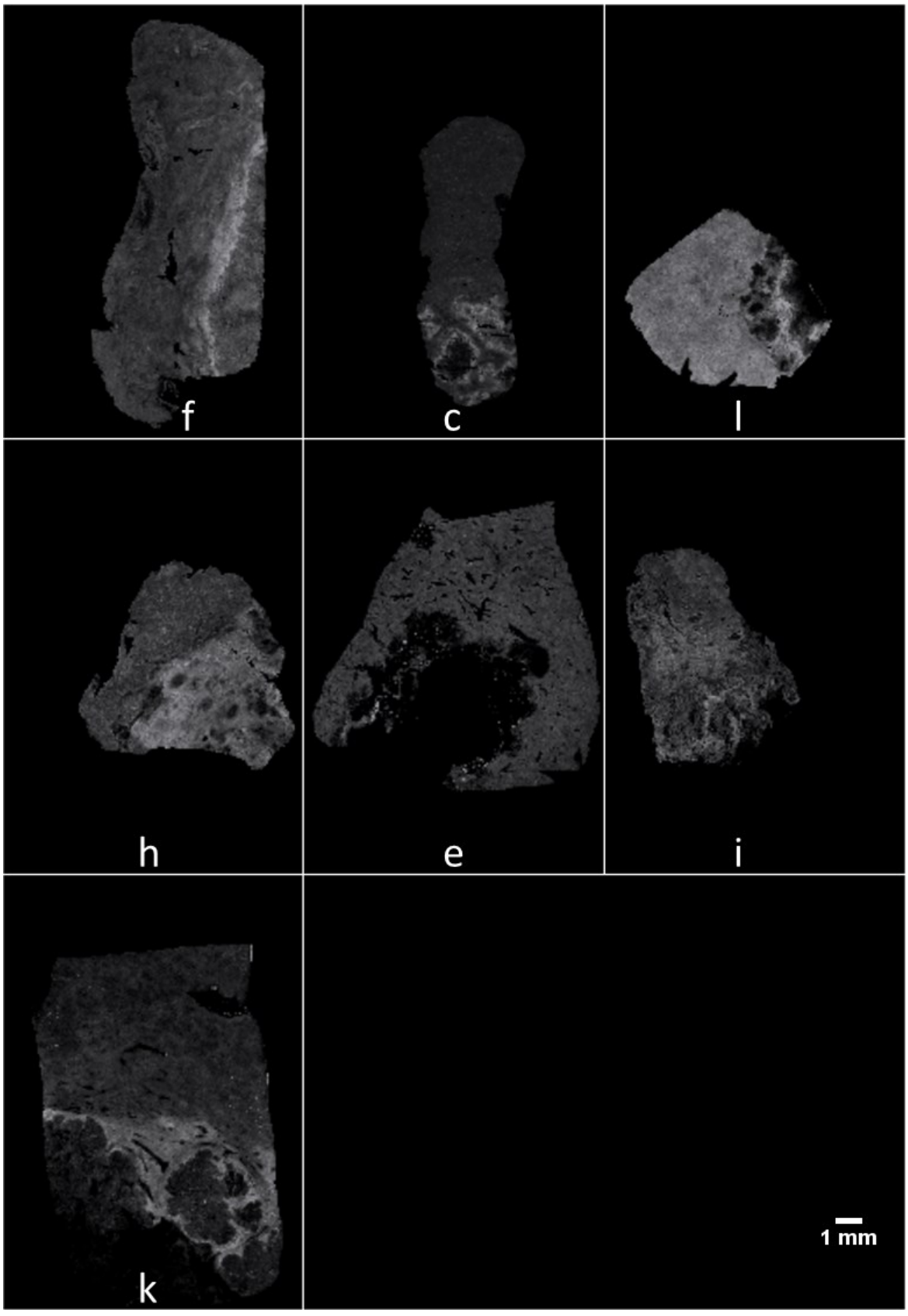

III. Markers of fibrotic tissue (grey), positive ionization mode. Grey = + *m/z* 782.55, PC(34:1) + K^+.

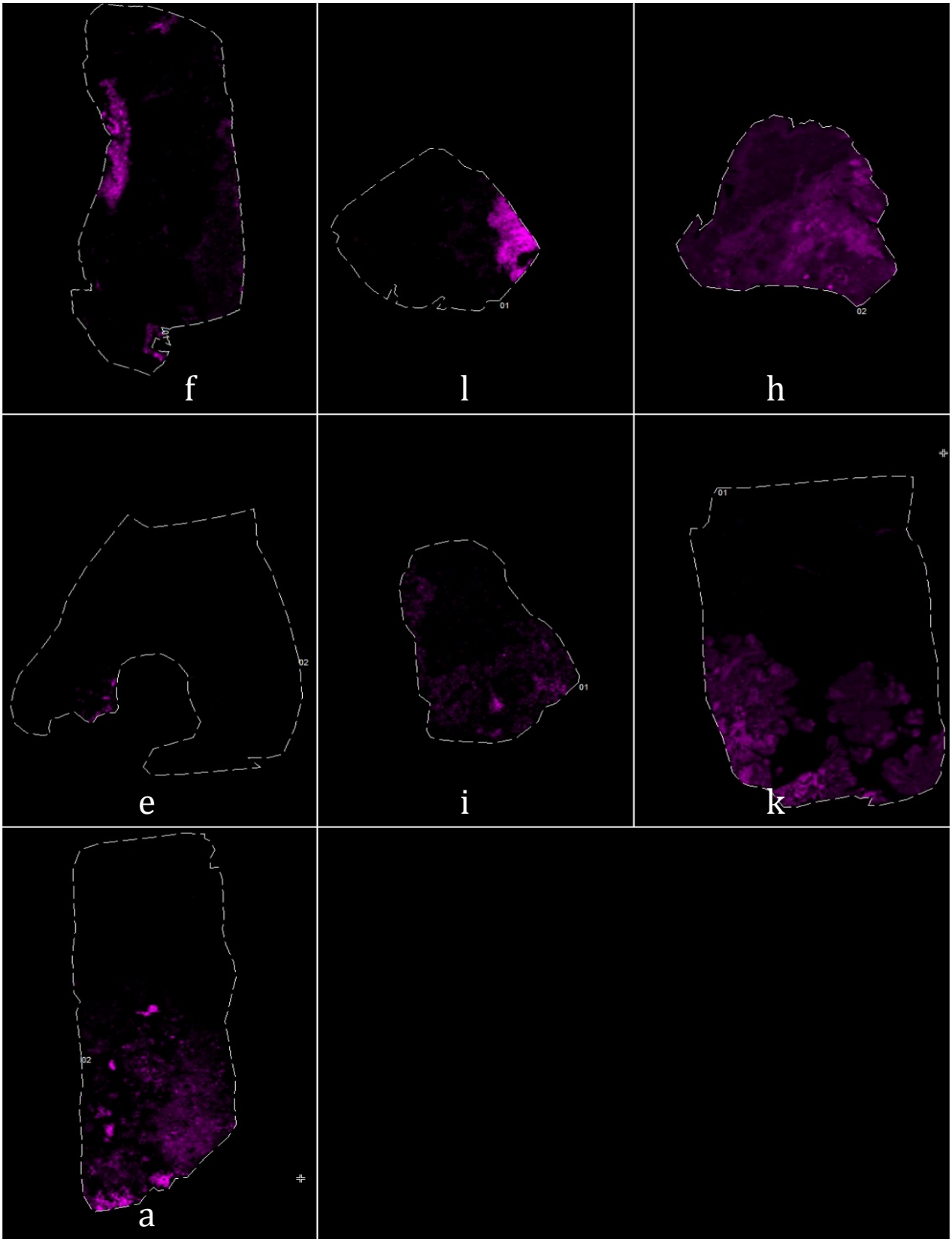

IV. Markers of necrotic tissue (purple), positive ionization mode. Purple = + *m/z* 703.55, SM(34:1). Outline of tissues highlighted with dotted line.